Eddy covariance data reveal that a small freshwater reservoir emits a substantial amount of carbon dioxide and methane

Alexandria G Hounshell[1,1], Brenda M D'Acunha[2,2], Adrienne Breef-Pilz[1,1], Mark S. Johnson[2,2], R. Quinn Thomas[1,1], and Cayelan Carey[1,1]

[1]Virginia Tech
[2]University of British Columbia

December 13, 2022

Abstract

Small freshwater reservoirs are ubiquitous and likely play an important role in global greenhouse gas (GHG) budgets relative to their limited water surface area. However, constraining annual GHG fluxes in small freshwater reservoirs is challenging given their footprint area and spatially and temporally variable emissions. To quantify the GHG budget of a small (0.1 km^2) reservoir, we deployed an eddy covariance system in a small reservoir located in southwestern Virginia, USA over two years to measure carbon dioxide (CO_2) and methane (CH_4) fluxes near-continuously. Fluxes were coupled with *in situ* sensors measuring multiple environmental parameters. Over both years, we found the reservoir to be a large source of CO_2 (633-731 g CO_2-C m^{-2} yr^{-1}) and CH_4 (1.02-1.29 g CH_4-C m^{-2} yr^{-1}) to the atmosphere, with substantial sub-daily, daily, weekly, and seasonal timescales of variability. For example, fluxes were substantially greater during the summer thermally-stratified season as compared to the winter. In addition, we observed significantly greater GHG fluxes during winter intermittent ice-on conditions as compared to continuous ice-on conditions, suggesting GHG emissions from lakes and reservoirs may increase with predicted decreases in winter ice-cover. Finally, we identified several key environmental variables that may be driving reservoir GHG fluxes at multiple timescales, including, surface water temperature and thermocline depth followed by fluorescent dissolved organic matter. Overall, our novel year-round eddy covariance data from a small reservoir indicate that these freshwater ecosystems likely contribute a substantial amount of CO_2 and CH_4 to global GHG budgets, relative to their surface area.

Eddy covariance data reveal that a small freshwater reservoir emits a substantial amount of carbon dioxide and methane

Alexandria G. Hounshell[1, †], Brenda M. D'Acunha[2], Adrienne Breef-Pilz[1], Mark S. Johnson[2,3], R. Quinn Thomas[1,4], Cayelan C. Carey[1]

[1] Department of Biological Sciences, Virginia Tech, Blacksburg, VA, USA, [2] Department of Earth, Ocean, and Atmospheric Sciences, University of British Columbia, Vancouver, BC, Canada, [3] Institute for Resources, Environment and Sustainability, University of British Columbia, Vancouver, BC, Canada, [4] Department of Forest Resources and Environmental Conservation, Virginia Tech, Blacksburg, VA, USA

Corresponding author: Alexandria G. Hounshell (alexgh@vt.edu)

† Current affiliation: National Centers for Coastal Ocean Science, National Oceanographic and Atmospheric Administration, Beaufort, NC, 28516 alexandria.hounshell@noaa.gov

Key Points:

- We measured high annual CO_2 and CH_4 fluxes over 2 years from a small reservoir
- Fluxes were higher in the summer than winter, with statistically higher fluxes during intermittent ice-on as compared to continuous ice-on
- Surface water temperature, thermocline depth, and dissolved organic matter concentrations were correlated with reservoir fluxes

Abstract

Small freshwater reservoirs are ubiquitous and likely play an important role in global greenhouse gas (GHG) budgets relative to their limited water surface area. However, constraining annual GHG fluxes in small freshwater reservoirs is challenging given their footprint area and spatially and temporally variable emissions. To quantify the GHG budget of a small (0.1 km^2) reservoir, we deployed an eddy covariance system in a small reservoir located in southwestern Virginia, USA over two years to measure carbon dioxide (CO_2) and methane (CH_4) fluxes near-continuously. Fluxes were coupled with *in situ* sensors measuring multiple environmental parameters. Over both years, we found the reservoir to be a large source of CO_2 (633-731 g CO_2-C m^{-2} yr^{-1}) and CH_4 (1.02-1.29 g CH_4-C m^{-2} yr^{-1}) to the atmosphere, with substantial sub-daily, daily, weekly, and seasonal timescales of variability. For example, fluxes were substantially greater during the summer thermally-stratified season as compared to the winter. In addition, we observed significantly greater GHG fluxes during winter intermittent ice-on conditions as compared to continuous ice-on conditions, suggesting GHG emissions from lakes and reservoirs may increase with predicted decreases in winter ice-cover. Finally, we identified several key environmental variables that may be driving reservoir GHG fluxes at multiple timescales, including, surface water temperature and thermocline depth followed by fluorescent dissolved organic matter. Overall, our novel year-round eddy covariance data from a small reservoir indicate that these freshwater ecosystems likely contribute a substantial amount of CO_2 and CH_4 to global GHG budgets, relative to their surface area.

Plain Language Summary

Freshwater ecosystems release substantial amounts of greenhouse gases, especially carbon dioxide and methane, to the atmosphere. Small waterbodies, such as lakes and reservoirs, are common in the landscape and may release particularly high levels of greenhouse gases, though their overall contribution remains unknown. The most common methods to date for estimating greenhouse gas emissions from freshwaters typically involve only measuring concentrations during the daytime on a handful of days throughout the year. Thus, there is a clear need for near-continuous measurements of carbon dioxide and methane from small waterbodies throughout the year on multiple timescales (hours to years). To do this, we measured fluxes of carbon dioxide

and methane from a small reservoir using eddy covariance over two years. We found this small reservoir to be a large source of both carbon dioxide and methane to the atmosphere over two years and found high variability in fluxes measured at short (sub-daily) to long (seasonal) timescales. Overall, this study demonstrates the importance of small reservoirs as greenhouse gas sources to the atmosphere and emphasizes the need for additional measurements to estimate their contribution to global greenhouse gas budgets.

1 Introduction

Freshwater ecosystems play a disproportionately large role in global greenhouse gas (GHG) budgets relative to their total water surface area, emitting more GHGs across all freshwaters than are taken up by global terrestrial ecosystems (Bastviken et al. 2011; Cole et al. 2007; DelSontro et al. 2018; Tranvik et al. 2009). Despite their importance, however, the contribution of inland waters, especially small (<1 km^2) reservoirs, remains under-represented within global carbon (C) and GHG budgets (Butman et al. 2018; Deemer and Holgerson, 2021; Deemer et al. 2016; DelSontro et al. 2018). It is estimated that there are ~5.8 million lakes and reservoirs in the contiguous U.S. (Winslow et al. 2014), of which approximately half (~2.6 million) are human-made reservoirs (Smith et al. 2002). Of these human-made reservoirs, small reservoirs (<1 km^2) compose >71% of reservoirs in the United States (National Inventory of Dams, USACE 2021), indicating that these ecosystems are extremely common, with at least ~1.8 million small reservoirs in the conterminous U.S.

Despite their ubiquity, constraining annual GHG estimates in small freshwater reservoirs is challenging given their small footprint area and heterogeneous GHG emissions (Loken et al. 2019; McClure et al. 2020; Podgrajsek et al. 2015). Short-term measurements indicate the potential for these ecosystems to exhibit high, but patchy fluxes (Deemer and Holgerson, 2021; DelSontro et al. 2018; McClure et al. 2018, 2020; Rosentreter et al. 2021), but to the best of our knowledge, their annual emissions remain largely unknown. To date, most studies measuring GHG emissions from freshwater lakes and reservoirs are based on snapshot measurements from short-term floating chamber deployments or grab samples of dissolved GHGs, which are extrapolated to broad spatial and temporal scales to estimate annual whole-ecosystem fluxes

(Bastviken et al. 2015; Klaus et al. 2019; Wik et al. 2016). While these approaches have provided useful insights into general patterns of GHG cycling in freshwater ecosystems, they are inherently limited in capturing the high spatial and temporal variability in freshwater GHG fluxes (A.K. Baldocchi et al. 2020; Butman et al. 2018; Klaus et al. 2019; Rosentreter et al. 2021; Wik et al. 2016).

Eddy covariance (EC) systems are increasingly being deployed on lakes and reservoirs to constrain sub-daily GHG fluxes over large spatial footprints, enabling the quantification of whole-ecosystem GHG fluxes at multiple temporal scales (e.g., A.K. Baldocchi et al. 2020; Golub et al. 2021; Eugster et al. 2011; Vesala et al. 2011; Waldo et al. 2021). EC systems are used to determine the net exchange of carbon dioxide (CO_2), methane (CH_4), and/or other gases at sub-hourly time scales via micrometeorology and *in situ* atmospheric trace gas concentrations measured using infrared gas analyzers (A.K. Baldocchi et al. 2020; Golub et al. 2021; Vesala et al. 2011). By collecting near-continuous, high frequency data (typically measured at 10-20 Hz and reported as 30-minute means), EC systems allow GHG fluxes to be estimated at sub-daily to annual timescales, improving our understanding of GHG flux temporal variability beyond traditional discrete measurements (Golub et al. 2021; Reed et al. 2018; Vesala et al. 2011). Additionally, EC systems often capture a larger spatial footprint compared to traditional discrete measurements, as measured fluxes represent the average flux from the atmospherically-mixed area upwind of the deployed EC system (Golub et al. 2021, Waldo et al. 2021). Thus, EC systems can greatly increase the temporal resolution and spatial extent of measured fluxes in lakes and reservoirs, with the caveat that important considerations and data filtering are needed for EC systems in small waterbodies (Scholz et al. 2021). Specifically, a waterbody's small surface area increases the likelihood of surrounding terrestrial vegetation impacting EC measurements of aquatic fluxes and decreases the area available for a well-mixed, turbulent footprint (Esters et al. 2020; Scholz et al. 2021; Vesala et al. 2011).

While the majority of reported freshwater EC studies have been conducted on short timescales (days to months; e.g., Erkkiliä et al. 2018; Gorsky et al. 2021; Jammet et al. 2015; Podgrajsek et al. 2014, 2015; Vesala et al. 2006, 2011), longer-term studies measuring CO_2 or CH_4 fluxes in lakes and reservoirs on annual timescales are becoming more common (e.g., A.K. Baldocchi et al. 2020; Golub et al. 2021; Huotari et al. 2011; Jammet et al. 2017; Liu et al. 2016; Reed et al. 2018; Shao et al. 2015; Scholz et al. 2021; Taoka et al. 2020; Waldo et al. 2021). An

annual study conducted in Lake Erie, USA found this highly-eutrophic system was a small sink of CO_2 during the summer productive season yet ultimately a CO_2 source on annual timescales (Shao et al. 2015). Other studies have highlighted the importance of short (hourly to daily), episodic events on annual CO_2 budgets, including the disproportionate effect of storms on annual CO_2 emissions from a large subtropical reservoir (Liu et al. 2016), fall mixing in a large (40 km^2) temperate lake (Reed et al. 2018), and pulses of CH_4 following ice-off in a north temperate lake (Gorsky et al. 2021). Studies conducted in the high northern latitudes during continuous ice-on conditions in winter observed zero to very low greenhouse gas fluxes from frozen lakes due to thick ice cover, which prevented the exchange of gasses across the air-water interface (e.g., Huotari et al. 2011; Jammet et al. 2017). In more temperate climates, other studies found low and relatively consistent CO_2 fluxes during continuous or intermittent ice-covered winter periods (A.K. Baldocchi et al. 2020; Reed et al. 2018). In addition to noted diel, seasonal, and episodic variability in CO_2 fluxes, two annual studies recently found the sub-monthly timescale to be an important timescale of variability, though the mechanism for this variability remains unknown (A.K. Baldocchi et al. 2020; Golub et al. 2021). Altogether, despite the increase in studies using EC systems to measure CO_2 and CH_4 fluxes from freshwaters, few studies to date have captured *both* CO_2 and CH_4 fluxes on the annual scale, especially during winter.

Measuring annual-scale CO_2 and CH_4 fluxes is particularly important as GHG fluxes are likely rapidly changing due to altered climate (Bartosiewicz et al. 2019; Beaulieu et al. 2019), motivating several potential hypotheses for how different environmental drivers may alter fluxes. Multiple environmental drivers sensitive to climate change likely affect GHG fluxes, though annual-scale studies to test the effects of these drivers on fluxes across multiple timescales are lacking. For example, increasing surface water temperatures and changes in precipitation and nutrient loading are changing phytoplankton productivity and allochthonous C inputs to lakes and reservoirs (Fowler et al. 2020; Hanson et al. 2015; Tranvik et al. 2009). For example, changes in freshwater primary production and nutrient inputs to freshwater systems have been directly linked to increases in CO_2 (DelSontro et al. 2018), as well as CH_4 emissions (Deemer and Holgerson, 2021; DelSontro et al. 2018; McClure et al. 2020). Finally, increasing air temperatures are leading to warmer winters and more intermittent and partial ice cover (Imrit and Sharma, 2021; Sharma et al. 2021; Woolway et al. 2020), allowing for potentially greater exchange of GHGs across the air-water interface, highlighting the need to understand the role of

ice in constraining GHG fluxes. All these examples emphasize the importance of measuring near-continuous GHG fluxes on the annual scale along with key potential environmental drivers, such as precipitation and freshwater inflows, surface water temperature, chlorophyll-*a*, dissolved organic matter, and ice-on/ice-off as potential GHG drivers, as it is likely that some drivers may have a greater effect at certain timescales than others.

Altogether, there is a clear need to measure annual-scale CH_4 and CO_2 fluxes from small freshwater ecosystems, especially small reservoirs. While several studies have measured annual CO_2 fluxes from freshwaters (e.g., A.K. Baldocchi et al. 2020; Golub et al. 2021; Huotari et al. 2011; Liu et al. 2016; Reed et al. 2018; Shao et al. 2015; Scholz et al. 2021), to the best of our knowledge, only one freshwater study has measured *both* CH_4 and CO_2 fluxes on an annual timescale (Jammet et al. 2017), while Taoka et al. (2020) and Waldo et al. (2021) measured only CH_4 fluxes at the annual scale. Specifically, Waldo et al. (2021) used EC to measure annual CH_4 fluxes from a large (2.4 km^2), highly-eutrophic temperate reservoir, measuring emissions up to 71.4 g CH_4 m^{-2} yr^{-1}, which is in the top quarter of those reported from lakes and reservoirs to date. In an Arctic lake, Jammet et al. (2017) used EC to measure low GHG fluxes during the winter ice-covered period, followed by large CH_4 and CO_2 fluxes during spring-thaw, and increasing ebullitive CH_4 fluxes during the ice-free season concurrent with small rates of CO_2 uptake during the summer due to photosynthesis. Aggregated across the full year, this Arctic lake was a net source of both CH_4 and CO_2 to the atmosphere (Jammet et al. 2017). Across the literature, most EC studies have focused on naturally-formed lakes, and all EC reservoir studies of which we are aware (Eugster et al. 2011; Golub et al. 2021; Liu et al., 2016; Waldo et al. 2021) were conducted in large (>2.4 km^2) reservoirs.

To better understand the GHG budgets of small reservoirs and the response of fluxes to key environmental drivers, we deployed an EC system in a small (0.1 km^2) freshwater reservoir located in southwestern Virginia, USA for two years to measure *both* CO_2 and CH_4 fluxes near-continuously. Flux measurements were coupled with *in situ* sensors measuring multiple environmental parameters, including surface water temperature, dissolved oxygen, chlorophyll-*a*, and fluorescent dissolved organic matter. Ultimately, we used the measured GHG fluxes and environmental variables to answer the questions: 1) What is the annual phenology of CO_2 and CH_4 fluxes in a small, eutrophic reservoir, including during the critical winter period?; and 2) Which environmental variables best explain CO_2 and CH_4 variability at daily to monthly

timescales? We expected CO_2 and CH_4 fluxes would be variable throughout the year, especially during the summer months, when we expected larger GHG fluxes and marked diel patterns following elevated primary production during the daylight hours. Conversely, during the winter months, we expected relatively low fluxes due to suppressed biological activity and potential ice-cover. Following these expectations, we predicted temperature would be an important environmental predictor positively-related to both CO_2 and CH_4, while chlorophyll-*a* would likely be an important environmental predictor positively related to CO_2 fluxes on multiple timescales.

2 Materials and Methods

2.1 Site description

Falling Creek Reservoir (FCR) is a small, eutrophic reservoir located in Vinton, Virginia, USA constructed in 1898 (Fig. 1; 37.303^{o}N, 79.837^{o}W; Gerling et al. 2016; Howard et al. 2021). The reservoir is located in a valley at 520 m above sea level. Hills on either side of the reservoir have a maximum elevation of 615 m (east) and 740 m (west) above sea level. The reservoir and surrounding forested watershed are owned and operated by the Western Virginia Water Authority (WVWA) as a primary drinking water source (Gerling et al. 2016). FCR has a surface area of 0.119 km^2 and a maximum depth of 9.3 m (McClure et al. 2018). The reservoir is dimictic and thermally stratified from April to October (McClure et al. 2018). During the study period, water was not extracted for drinking water treatment and remained at a constant full-pond level. The water residence time during the study period ranged from 21 to 635 d, with a median of 247 d (Fig. S1; calculated using the methods of Gerling et al. 2014). Since the reservoir remained at full pond, we assumed incoming discharge from the primary inflow was equal to outflowing discharge during the two-year study period.

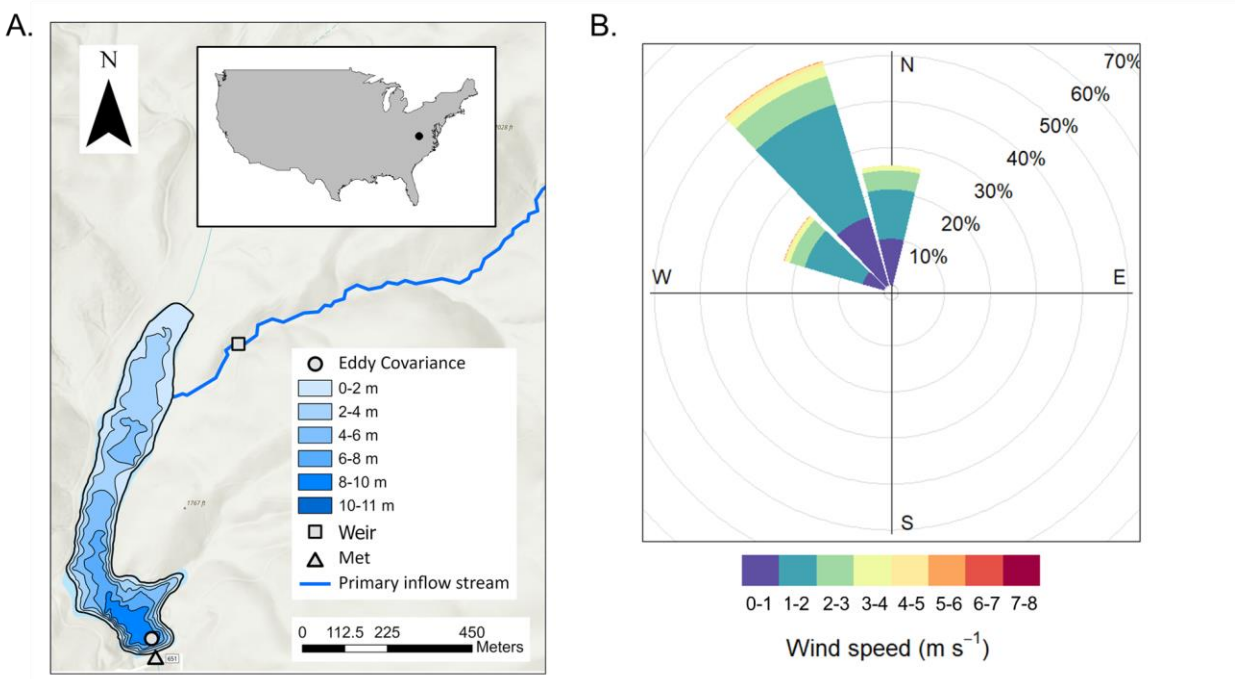

Figure 1. A. Map of Falling Creek Reservoir (FCR) located in Vinton, Virginia, USA (map inset) showing location of the eddy covariance system, the weir located on the primary freshwater inflow, and the meteorological station located on the dam. B. Wind rose showing the dominant wind direction and wind speed (m s^{-1}) of greenhouse gas fluxes retained for analysis. The cumulative footprint distribution for the study period is shown in the supplementary information (Fig. S2).

2.2 Data collection and overview

We used an EC system deployed near the dam on an existing metal platform extending into the reservoir to measure CO_2 and CH_4 fluxes between the water surface and the atmosphere from 1 May 2020 to 30 April 2022 (details below; Carey et al. 2022a). To complement the EC measured fluxes, we also calculated CO_2 and CH_4 diffusive gas fluxes using dissolved CO_2 and CH_4 discrete grab samples collected during daylight hours (between ~08:00 to 13:00) weekly to monthly from the water's surface at the deepest site of the reservoir, located near the dam, throughout the 2-year study period (details below; Carey et al. 2022b). The EC system was co-located near the reservoir dam to take advantage of the existing limnological and meteorological suite of instruments already deployed at this location as well as existing electrical power and infrastructure for EC deployment.

In addition to the EC and diffusive fluxes, we also collected meteorological and environmental data. Briefly, a Campbell Scientific (Logan, Utah, USA) research-grade

meteorological station measured air temperature; relative humidity; air pressure; wind speed and direction; upwelling and downwelling shortwave and longwave radiation; total rainfall; photosynthetically-active radiation (PAR); and albedo every minute at the reservoir dam (sensor information provided by Carey et al. 2022c). At the reservoir's deepest site, we collected 10-minute water temperature measurements every 1 m from the surface (0.1 m) to just above the sediments (9 m) using a thermistor string. Thermistor data were used to calculate the difference in temperature between 0.1 m and 9.0 m (Diff. Temp) and daily buoyancy frequency (N^2), two metrics of thermal stratification, as well as thermocline depth throughout the study period (May 2020 to April 2022) using the LakeAnalyzer package in R (Winslow et al. 2016a). Fall turnover was defined as the first day in autumn when the temperature at 1 m was $<1^oC$ of the temperature measured at 8 m (1 November 2020 and 3 November 2021; McClure et al. 2018). Spring mixing was harder to identify due to intermittent ice-on in 2021 and frequent mixing during the winter period, but we defined spring mixing as the first day in spring after complete ice-off when the temperature at 1 m was $<1^oC$ of the temperature measured at 8 m (26 February 2021 and 10 February 2022). For 2022, spring mixing occurred on the same day as complete ice-off. Ice cover was determined by the presence of inverse stratification coupled with higher albedo and verified by visual observation, described by Carey and Breef-Pilz (2022).

Water column temperature data complemented 10-minute measurements of dissolved oxygen (DO) percent saturation, chlorophyll-*a* (Chl-*a*, µg L^{-1}), and fluorescent dissolved organic matter (fDOM, relative fluorescent units, RFU) measured using an EXO2 sonde (YSI, Yellow Springs, Ohio, USA) deployed at 1.6 m (Carey et al. 2022d), which is the depth historically used for water extraction when the reservoir is in-use (Howard et al. 2021). The EXO2 sonde was removed from the reservoir on 2 December 2020 for annual sensor maintenance and re-deployed on 27 December 2020. Finally, we measured stream inflow every 15 minutes on the primary inflowing stream to the reservoir via a gaged v-notch weir fitted with a Campbell Scientific CS451 pressure transducer (Campbell Scientific, Logan, Utah, USA), which was used to calculate the 15-minute flow rate following Carey et al. (2022e). The weir was breached on 20 July 2020 and repaired on 24 August 2020, resulting in no flow data during this interval.

2.3 Eddy covariance flux measurements

An EC system was deployed above the water surface over the deepest portion of the reservoir from 1 May 2020 to 30 April 2022. The EC instrumentation was installed 2.9 m over the reservoir's surface on a permanent metal platform that extends ~45 m from the dam. As noted above, the reservoir was maintained at full pond, resulting in a consistent height of the EC system over the water's surface during the study period. The placement of the EC sensors at 2.9 m above the water surface reflects a balance between ensuring adequate frequency responses to capture eddies (Burba and Anderson, 2010) and capturing a flux footprint that represents the area of interest. This height resulted in a flux footprint that was generally well matched to the reservoir (Fig. S2).

The EC system included an ultrasonic anemometer to measure 3D wind speed and direction (CSAT3, Campbell Scientific), an open-path infrared gas analyzer for measuring CH_4 concentration (LI-7700, LiCor Biosciences, Lincoln, Nebraska, USA), and an enclosed-path infrared gas analyzer for measuring CO_2 and water vapor concentrations (LI-7200, LiCor Biosciences), all recorded at 10 Hz by a data logger (LI-7550, LiCor Biosciences). On 10 August 2020, the data logger was removed for maintenance and re-deployed on 2 September 2020. Additionally, a thermocouple on the CO_2 sensor (LI-7200) was inoperable starting on 5 April 2021 and was repaired on 26 April 2021.

The raw 10-Hz data were first processed into 30-minute fluxes using the EddyPro v.7.0.6 software (LiCor Biosciences 2019). Fluxes were calculated following standard methods in EddyPro v.7.0.6 (LiCor Biosciences 2019), which included spike detection and removal (Vickers and Mahrt, 1997), a double rotation for tilt correction (Lee et al. 2005), linear detrending (Gash and Culf, 1996), time lag compensation, and spectral corrections for high and low-pass filtering effects following Moncrieff et al. (2004) and Moncrieff et al. (1997), respectively. In addition, CH_4 molar density was corrected to account for air density fluctuations and spectroscopic effects of temperature, pressure and water vapor (McDermitt et al. 2011; Webb et al. 1980). This correction was not needed for CO_2, as fluxes were estimated using mixing ratios instead of densities (Burba et al. 2012).

Following initial flux calculations and processing in EddyPro, we conducted additional data processing following standard best practices, including: 1) removing wind directions which originated outside of the reservoir (80-250°; Fig. 1); 2) removing extreme flux values (CO_2 fluxes ≥ |100| μmol C m^{-2} s^{-1}; CH_4 fluxes ≥ |0.25| μmol C m^{-2} s^{-1}); 3) removing CH_4 fluxes when signal strength <20%; 4) removing CO_2 and CH_4 fluxes when they did not pass the test for stationarity or developed turbulent conditions (QC, quality control level 2 per Mauder and Foken, 2006), in addition to when the latent heat (LE) or sensible heat flux (H) had QC level <2; 5) removing open-path CH_4 fluxes during periods of rainfall, which was determined based on the rain gauge deployed at the dam; 6) removing additional periods of low turbulence friction velocity (u_*), as described below; and 7) removing data that corresponded to flux footprints that extended significantly beyond the reservoir. We used REddyProc (Wutzler et al. 2021) to determine the u_* threshold for sufficiently turbulent conditions and removed any fluxes where u_* was < 0.075 m s^{-1}. To account for the uncertainty of estimating the u_* threshold, we used bootstrapping to estimate the distribution of u_* thresholds, and obtained the 5^{th}, 50^{th} and 95^{th} percentiles of this distribution (0.070, 0.075, and 0.163 m s^{-1}, respectively; Wutzler et al., 2018).

The final filtering step consisted of removing fluxes that extended beyond the reservoir. To do that, flux footprints were modeled for each half-hour using a simple, two-dimensional parameterization developed by Kljun et al. (2015) (Fig. S2). This model builds on the Lagrangian stochastic particle dispersion model (Kljun et al. 2002), and provides information on the extent, width, and shape of the footprint. All the variables needed for the model were obtained directly from the dataset described above or calculated following Kljun et al. (2015). Fluxes were excluded when the along-wind distance providing 90% cumulative contribution to turbulent fluxes was outside the reservoir, based on the footprint analysis. We chose to use this filtering threshold given the challenges of modeling footprints in small reservoirs; consequently, our fluxes are likely conservative. All post-processing analyses were conducted using R statistical software (v.4.0.3). Code for post-processing and all EC data can be found in the Environmental Data Initiative (EDI) repository (Carey et al. 2022a).

Overall, EC measurements captured 23% and 19% of total CO_2 and CH_4 fluxes, respectively, over two years from FCR (Table S1), which is similar to previously-reported deployments of EC systems at lakes and reservoirs (e.g., Golub et al. 2021; Reed et al. 2018;

Waldo et al. 2021). The percentage of available data was relatively consistent across half-hourly periods (from 00:00 to 23:30), ranging from 14%-34% of data availability for CO_2 for 22:00 and 12:30 half-hourly periods, respectively, and 11%-32% for CH_4 (22:00 and 12:30 half-hourly periods, respectively; Fig. S3). We note that during the day, the dominant wind direction was outside the reservoir footprint, while the dominant wind direction was largely along the reservoir at night (Fig. S4). This pattern resulted in a high percentage of daytime fluxes removed due to wind direction, but overall, we observed a roughly equal contribution of day and night fluxes following all flux removal processes (i.e., flux filtering due to low u*). Data availability after filtering was also relatively consistent throughout seasons and between years, ensuring even representation of measured fluxes throughout the year (Fig. S5). We do note low data availability (<10%) for both CO_2 and CH_4 fluxes during August 2020, due to instrument maintenance, and for CH_4 during December 2020 and February 2021 due to issues with instrument power stability.

2.4 Diffusive flux measurements

We estimated discrete diffusive fluxes from FCR using dissolved CO_2 and CH_4 samples (Carey et al. 2022b) collected at the surface of the reservoir to compare with EC fluxes. Surface water samples were collected at 0.1 m depth using a 4-L Van Dorn sampler (Wildlife Supply Co., Yulee, Florida, USA) adjacent to the EC sensors (Fig. 1). Replicate (n=2) water samples were collected via a Van Dorn sampler into 20-mL serum vials without headspace, immediately capped, and then stored on ice until analysis within 24 hours. Prior to sample analysis, a small amount of water was removed from each sample and replaced with a neutral gas (helium gas). Samples were analyzed following Carey et al. (2022b) on a Shimadzu Nexis GC-2030 Gas Chromatograph (Kyoto, Japan) with a Flame Ionization Detector (GC-FID) and Thermal Conductivity Detector (TCD).

The measured surface samples were used to calculate CO_2 and CH_4 diffusive fluxes from the surface of FCR into the atmosphere on each day of sample collection following the equation:

$$Flux = k * (C_{water} - C_{eq}) \quad \text{Eq. 1}$$

where k is the temperature-corrected gas transfer velocity (m d^{-1}) for the gas species (CO_2 or CH_4, respectively), and $(C_{water} - C_{eq})$ is the dissolved gas concentration in excess of

atmospheric concentrations (Cole and Caraco, 1998; Wanninkhof et al. 2009). C_{water} is the concentration (mass volume^{-1}) of CO_2 or CH_4 at the reservoir surface (0.1 m), and C_{eq} is the concentration of dissolved gas at equilibrium with the EC-measured atmospheric concentration of CO_2 or CH_4. The GHG flux value was calculated separately for each of the two dissolved GHG sample replicates collected at each time point using the seven k models included in the LakeMetabolizer package in R (Cole and Caraco, 1998; Crusius and Wanninkhof 2003; Heiskanen et al. 2014; MacIntyre et al. 2010; Read et al. 2012; Soloviev et al. 2007; Vachon and Prairie, 2013; Winslow et al. 2016b, 2016c). We report the mean and standard deviation from the n=14 replicate-model k determinations to account for uncertainty introduced through various k estimations. We feel this approach offers the best representation of potential diffusive flux values that can be directly compared to fluxes measured by EC (Erkkilä et al. 2018; Schubert et al. 2012).

2.5 Statistical analyses

To assess the phenology of fluxes (CO_2 and CH_4), we analyzed the mean and standard deviation (±1 S.D.) of measured EC fluxes at half-hourly, daily, weekly, and monthly time scales through the study period. For both EC and discrete diffusive fluxes, negative fluxes correspond to fluxes into the reservoir (i.e., uptake) while positive fluxes are out of the reservoir (i.e., release to the atmosphere).

To assess diel variation in GHG fluxes, we compared median measured EC fluxes during the day (11:00 to 13:00) and night (23:00 to 01:00) throughout the study period. As data were not normally distributed, we used paired Wilcoxon signed-rank tests to assess statistical significance of paired day-night fluxes ($\alpha = 0.05$). Additionally, we compared dawn (05:00 to 07:00) and dusk (17:00 to 19:00) median EC measured fluxes using the same methods.

Ice coverage at FCR is episodic and ephemeral, encompassing longer ice-covered periods as well as shorter-duration ice-covered periods when ice may be present during portions of sequential days or with partial coverage of the reservoir's surface, which we refer to as intermittent ice-on periods. To explore the role of variable winter ice cover on CO_2 and CH_4 fluxes, we analyzed mean half-hourly fluxes (±1 S.D.) from 10 January to 10 February for both 2021 and 2022, which encompassed a period of intermittent (2021) and continuous (2022) ice-on

(following Carey and Breef-Pilz 2022; Table S2). We used Mann-Whitney-Wilcoxon tests to determine statistically-significant differences ($\alpha = 0.05$) between the median half-hourly fluxes measured during intermittent and continuous ice-on periods.

Finally, we calculated the net annual flux balance for CO_2 and CH_4 using both measured and gap-filled half-hourly EC data. Briefly, after filtering, half-hourly fluxes were gap-filled in REddyProc using the marginal distribution sampling method (MDS), which uses the correlation of measured fluxes with environmental driver variables, namely, radiation, temperature, and vapor pressure deficit (VPD) to estimate fluxes during the missing time periods (Wutzler et al. 2018). Prior to MDS, we used the meteorological data measured at the dam to gap-fill any missing wind speed, direction, temperature, and relative humidity in the EC dataset (Table S3). Overlapping data show that all meteorological variables were tightly correlated between the EC system and the adjacent meteorological station (Pearson's rho=0.81-0.98; Table S3). Gap-filling was performed for each of the u* scenarios, providing information about the uncertainty that might be introduced to the data by choosing a u* threshold. Measured and gap-filled fluxes were summed across each year (01 May - 30 April). The standard deviation (±1 S.D.) was calculated for both the measured and gap-filled data using the different u* scenarios.

2.6 Time series analysis

To identify key environmental predictors and test mechanistic relationships between observed mean daily, weekly, and monthly measured CO_2 and CH_4 fluxes and environmental variables, we developed separate autoregressive integrated moving average (ARIMA) models for each timescale. ARIMA models are used to identify key environmental predictors while accounting for temporal autocorrelation (Hyndman and Athanasopoulos, 2018). We selected several potential, in-reservoir, environmental predictors, including: surface water temperature (Temp, 0.1 m, ^{o}C); the difference between surface (0.1 m) and bottom (9 m) water temperatures (Diff. Temp); buoyancy frequency (N^2); thermocline depth (TD); DO percent saturation (DO sat); Chl-*a*; fDOM; and discharge (Inflow) measured at the primary inflow to FCR (Fig. S6, S7). We chose to focus on limnological environmental variables to help identify potential drivers of GHG fluxes, following our predictions. Prior to ARIMA modeling, we conducted pairwise Spearman correlations on all predictor variables (aggregated to each time scale) and removed

collinear variables (Pearson's rho≥0.7) that were the least correlated with fluxes. N^2 and Diff. Temp were removed for all time scales due to their strong correlation with surface water temperature (Table S4). Response and predictor variables were checked for skewness, transformed if appropriate, and normalized (z-scores) prior to model fitting (Hounshell et al. 2022).

We used a model selection algorithm (Lofton et al. 2022) to identify the importance of environmental predictor variables at each time scale. The algorithm was based on the auto.arima function in the forecast package in R (Hyndman and Khandakar, 2008; Hyndman et al. 2021) which compared fitted models to a global model (all possible predictors) and a null persistence model with just one autoregressive term (AR(1)). We selected the environmental model with the lowest corrected Akaike information criterion (AICc), as well as models within 2 AICc units (Burnham and Anderson, 2002). Models were limited to include one autoregressive term (Hounshell et al. 2022).

3 Results

3.1 Phenology of CO_2 and CH_4 fluxes

High-frequency EC data show that FCR was generally a net source of both CO_2 and CH_4 to the atmosphere across multiple timescales (Figs. 2, 3, S7; Tables S5). Overall, measured CO_2 fluxes ranged from -39.46 to 52.67 μmol m^{-2} s^{-1} with a mean flux of 1.86 ± 6.21 μmol m^{-2} s^{-1} (±1 S.D.) aggregated over the entire 2-year study period. Measured CH_4 fluxes ranged from -0.084 to 0.096 μmol m^{-2} s^{-1}, with a mean CH_4 flux of 0.003 ± 0.011 μmol m^{-2} s^{-1} over the study period (Fig. 2, 3, S8; Table S5).

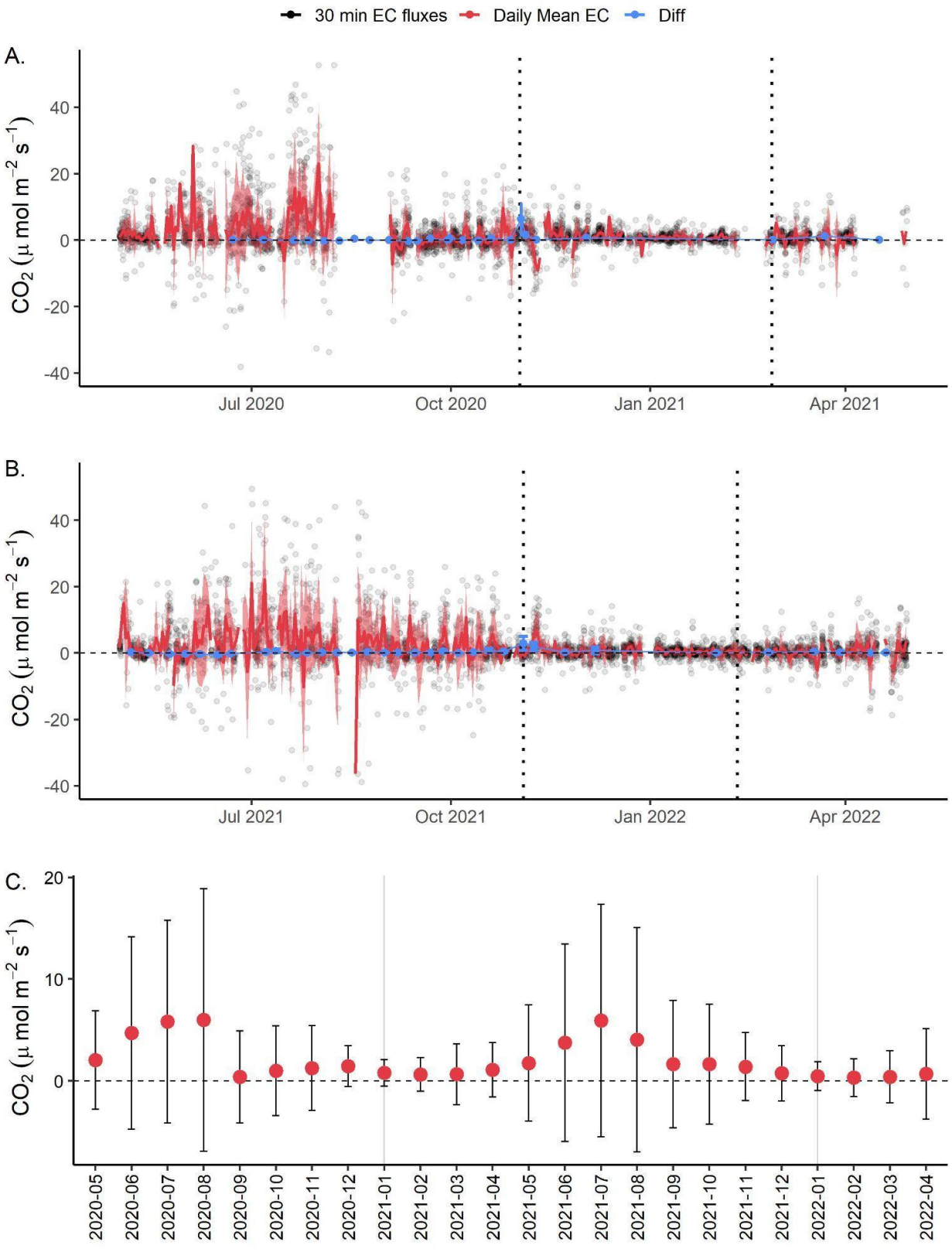
30 min EC fluxes
Daily Mean EC
Diff
A.
B.
C.
CO_2 (μ mol m^{-2} s^{-1})
40
20
0
-20
-40
Jul 2020
Oct 2020
Jan 2021
Apr 2021
Jul 2021
Oct 2021
Jan 2022
Apr 2022
10
2020-05
2020-06
2020-07
2020-08
2020-09
2020-10
2020-11
2020-12
2021-01
2021-02
2021-03
2021-04
2021-05
2021-06
2021-07
2021-08
2021-09
2021-10
2021-11
2021-12
2022-01
2022-02
2022-03
2022-04

409

Figure 2. Daily mean carbon dioxide fluxes (CO_2, μmol m^{-2} s^{-1}) for A. May 2020 to April 2021 (Year 1) and B. May 2021 to April 2022 (Year 2) measured using eddy covariance (Daily Mean EC, red) and calculated discrete diffusive fluxes (Diff, blue) using the mean and standard deviation of two replicate samples and seven gas transfer coefficient models (k; Winslow et al. 2016b). Grey dots represent measured half-hourly fluxes from the EC. The dark red line represents daily mean fluxes. The shaded red area represents ±1 standard deviation of the daily 30-minute fluxes using measured EC fluxes. The vertical dotted line indicates the onset of reservoir fall and spring mixing, respectively. C. Mean monthly CO_2 fluxes (μmol m^{-2} s^{-1}) aggregated from measured EC data. The error bars correspond to ±1 S.D. of aggregated fluxes for both measured and gap-filled EC values. The horizontal dashed line indicates zero fluxes.

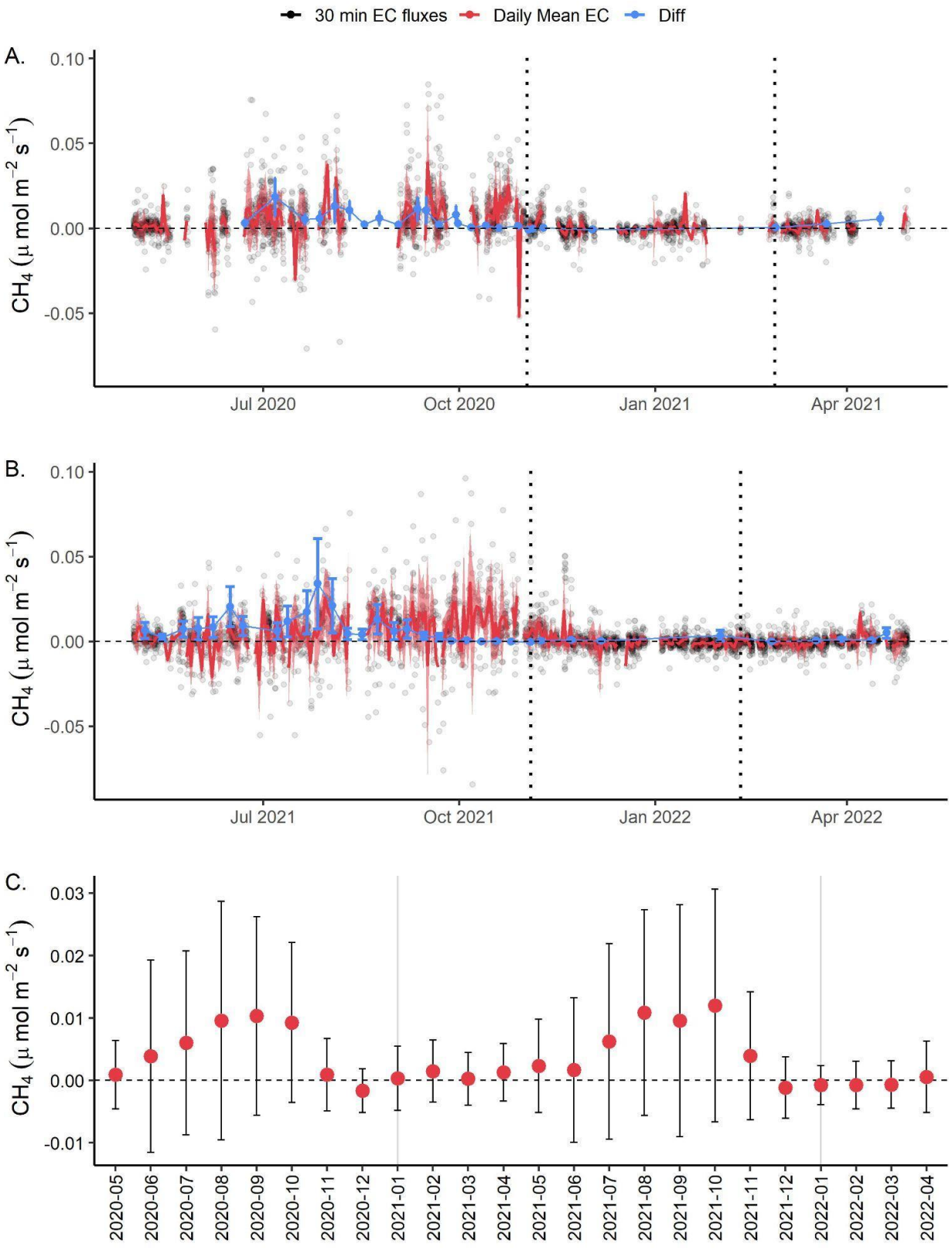
30 min EC fluxes
Daily Mean EC
Diff
A.
B.
C.
CH_4 (μ mol m^{-2} s^{-1})
0.10
0.05
0.00
-0.05
Jul 2020
Oct 2020
Jan 2021
Apr 2021
Jul 2021
Oct 2021
Jan 2022
Apr 2022
0.03
0.02
0.01
-0.01
2020-05
2020-06
2020-07
2020-08
2020-09
2020-10
2020-11
2020-12
2021-01
2021-02
2021-03
2021-04
2021-05
2021-06
2021-07
2021-08
2021-09
2021-10
2021-11
2021-12
2022-01
2022-02
2022-03
2022-04

420

Figure 3. Daily mean methane fluxes (CH_4, μmol m^{-2} s^{-1}) for A. May 2020 to April 2021 (Year 1) and B. May 2021 to April 2022 (Year 2) measured using eddy covariance (Daily Mean EC, red) and calculated discrete diffusive fluxes (Diff, blue) using the mean and standard deviation of two replicate samples and seven gas transfer coefficient models (k; Winslow et al. 2016b). Grey dots represent measured half-hourly fluxes from the EC. The dark red line represents daily mean fluxes. The shaded red area represents ±1 standard deviation of the daily 30-minute fluxes. The vertical dotted line indicates the onset of reservoir fall and spring mixing for each year, respectively. C. Mean monthly CH_4 fluxes (μmol m^{-2} s^{-1}) aggregated from measured EC data. The error bars correspond to ±1 S.D. of aggregated fluxes for both measured and gap-filled EC values. The horizontal dashed line indicates zero fluxes.

At the hourly to diel scale, we found that certain times of day had higher fluxes than others, but that overall, there was little difference in fluxes at midday versus midnight. Measured EC fluxes revealed no statistically significant difference between paired CO_2 fluxes measured during the day (11:00 to 13:00) as compared to night (23:00 to 01:00; p=0.09; Fig. 4; Table S6), and no statistically significant difference between paired, measured day and night CH_4 fluxes (p=0.16; Fig. 4; Table S6). We did observe significantly higher median CO_2 fluxes measured at dawn (05:00 to 07:00; 1.34 μmol m^{-2} s^{-1}) as compared to dusk (17:00 to 19:00; -0.030 μmol m^{-2} s^{-1}; p<0.001; Fig 4; Table S6), which may be related to higher median dawn wind speeds (p<0.001), though there was no statistical difference between dawn and dusk CH_4 fluxes.

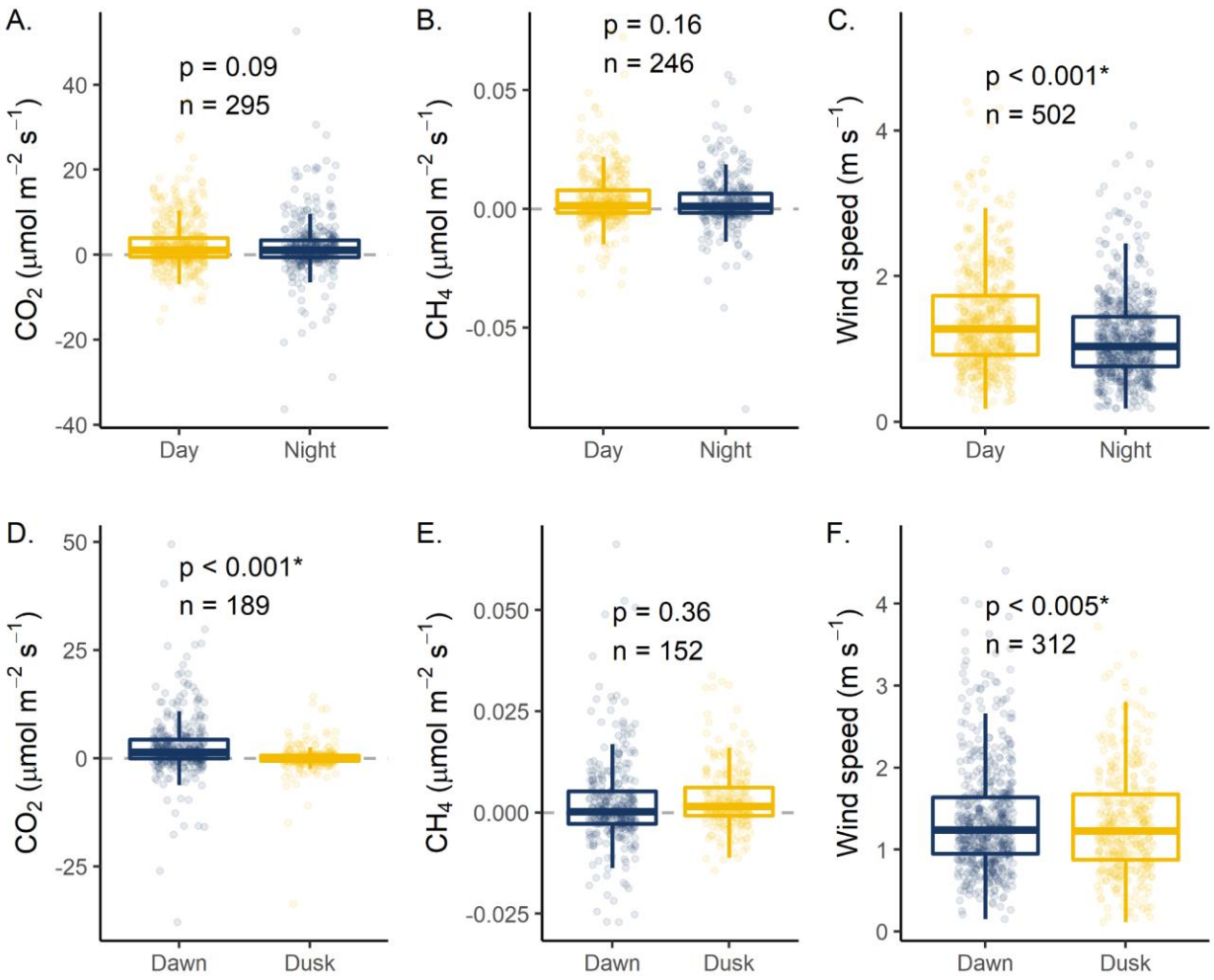

Figure 4. Day (11:00 to 13:00) vs. night (23:00 to 01:00) comparisons of A. carbon dioxide (CO_2, µmol m^{-2} s^{-1}) fluxes, B. methane (CH_4, µmol m^{-2} s^{-1}) fluxes, and C. wind speed (m s^{-1}) measured using the eddy covariance (EC) system deployed at Falling Creek Reservoir. Points represent measured half-hourly fluxes, while the boxes represent the 25th and 75th percentile, respectively and the thick line shows the median flux calculated with measured EC data. Dawn (05:00 to 07:00) vs. dusk (17:00 to 19:00) comparisons of D. CO_2 fluxes, E. CH_4 fluxes, and F. wind speed. Wilcoxon signed-rank tests were used to determine statistical significance between paired (day to night; dawn to dusk) fluxes. Statistical significance was defined a priori as $p<0.05$; asterisks indicate statistically significant differences. n indicates the number of paired fluxes (Table S6).

At the seasonal scale, both CO_2 and CH_4 fluxes (EC and diffusive measured fluxes) were greater in magnitude and more variable during the summer than winter, with increasing fluxes during the late spring and decreasing fluxes during the late fall (Figs. 2, 3). During the summer months (June – August), FCR was an overall source of CO_2 and CH_4 to the atmosphere for both

years (Figs. 2, 3). Specifically, CO_2 and CH_4 fluxes were up to 5× and 15× greater, respectively, during the summer stratified period (May – October) as compared to the winter and early spring (November – April; Fig. 2, 3, S9). During fall turnover, EC measured CO_2 fluxes remained low in both years (2020, 2021), while diffusive fluxes showed an increase in CO_2 fluxes on the day of turnover (Figs. 2, S11). Similarly, CH_4 fluxes were also low during and following turnover for both EC and diffusive fluxes in both years (Figs. 3, S9). From September to April, FCR was a small CO_2 source, but emitted less CO_2 than during the summer. For CH_4, FCR was almost net neutral from late fall to early spring (November to April), in contrast to larger CH_4 emissions during the summer. Following the onset of spring mixing, there was a small, but notable increase in CO_2 emissions in 2021 but little change in CH_4 emissions. In 2022, there were no notable changes in either CO_2 or CH_4 fluxes following ice-off and subsequent spring mixing in 2022 (Fig. 5). At the annual scale, there were notably higher CO_2 fluxes in the late-summer and early fall 2021 as compared to the summer and fall 2020, while for CH_4 fluxes, there were notably higher fluxes both in the mid-summer 2021 and in the late-summer and early fall 2021 (Figs. 2, 3).

3.2 Comparison of EC and diffusive fluxes

Overall, both CO_2 and CH_4, diffusive fluxes were within the range of measured EC fluxes, though diffusive CO_2 fluxes were lower than measured EC fluxes when comparing discrete timepoints (Fig. 2, 3; Table S5). Specifically, hourly CO_2 diffusive fluxes calculated from grab surface samples were an order of magnitude lower than measured EC fluxes and ranged from -1.24 to 17.50 μmol m^{-2} s^{-1}, with a mean flux of 0.39 ± 1.29 μmol m^{-2} s^{-1} (Figs. 2, S10, S11; Table S5). We note that the magnitude of diffusive fluxes was highly sensitive to the gas transfer coefficient method (k) used in flux calculations, and thus we presented the mean and standard deviation of the seven different k models used, which represent the range of possible diffusive fluxes which could be compared to EC measured fluxes (Eq. 1; Fig. S10). Hourly CH_4 diffusive fluxes were more comparable to measured EC fluxes, with a range of -0.003 to 0.096 μmol m^{-2} s^{-1} and a mean of 0.006 ± 0.009 μmol m^{-2} s^{-1} (Figs. 3, S10, S11; Table S5).

3.3 Environmental predictors of CO_2 and CH_4 fluxes

During the study period, FCR experienced typical meteorological and environmental conditions. The meteorology measured at the reservoir dam recorded a mean air temperature of 14.1°C (13.8 and 14.4°C in years 1 and 2, respectively), with a minimum and maximum temperature of -11.5 and 35.1°C, respectively across the two years (Table S7). Mean wind speed during the time period was 1.99 m s^{-1} (2.00 and 1.97 m s^{-1} for years 1 and 2, respectively), with a maximum wind speed of 11.2 m s^{-1} and a dominant wind direction of 198° (191° and 199° for years 1 and 2, respectively). Yearly total rainfall ranged from 790 mm (Year 2) to 1438 mm (Year 1). During the winter (January - February), air temperatures in year 1 ranged from -8.0 to 19.4°C with a mean of 1.9°C and in year 2 ranged from -11.5 to 21.4°C with a mean of 2.1°C.

Water column variables measured at 1.6 m below the surface also exhibited typical annual patterns and were for the most part similar between years. We found water temperatures ranged from 1.23 to 31.4°C, with a mean of 15.2 and 15.9°C for years 1 and 2, respectively (Fig. S6; Table S8). Chl-a values ranged from 0.25 to 121 μg L^{-1}, with a mean of 11.5 μg L^{-1} and 12.3 μg L^{-1} in years 1 and 2, respectively. fDOM was also nearly identical in years 1 and 2 with a mean of 6.09 and 6.04 RFU, respectively, and a range of 3.01 to 10.4 RFU. For DO sat., the mean was 107 and 97.8% in year 1 and year 2. Finally, inflow was higher in year 1 (0.056 m^3 s^{-1}) as compared to year 2 (0.013 m^3 s^{-1}) and ranged from 0.005 to 0.27 m^3 s^{-1} (Fig. S7; Table S8). This resulted in a substantial difference in calculated water residence time, with substantially lower mean water residence time in year 1 (148 ± 169 d) as compared to year 2 (347 ± 119 d; Fig. S1).

Overall, surface water temperature and thermocline depth were found to be the most important environmental predictors for both CO_2 and CH_4 fluxes over all timescales analyzed (daily, weekly, monthly), followed by fDOM (Table 1). Inflow discharge was only intermittently important for CO_2 and CH_4 fluxes at various timescales while DO sat. and Chl-a were only intermittently important for CO_2 fluxes (Tables 1, S9). Water temperature was positively correlated with both CO_2 and CH_4 fluxes at all timescales, following the pattern of higher GHG fluxes during summer as compared to winter in the time series data (Figs. 2, 3). CO_2 fluxes were negatively associated with thermocline depth while CH_4 fluxes were positively associated with

thermocline depth at all timescales (Table 1); i.e., CO_2 fluxes were greater when there were shallower thermocline depths, whereas CH_4 fluxes were greater when there were deeper thermocline depths.

In addition to water temperature and thermocline depth, CO_2 fluxes were positively associated with fDOM across all timescales, while CH_4 fluxes were only positively associated with fDOM at the daily and weekly timescales (Table 1). Conversely, inflow was positively associated with CO_2 fluxes at daily and weekly timescales, while inflow was negatively associated with CH_4 fluxes at weekly and monthly timescales. Finally, Chl-a was negatively associated with CO_2 fluxes, but only on the daily timescale and was negatively associated with DO sat. at the weekly timescale. CH_4 fluxes were not associated with either Chl-a or DO sat. at any timescale.

CO_2 fluxes were best predicted by ARIMA models at the monthly timescale (RMSE=0.48 μmol m^{-2} s^{-1}), with descending RMSE for the weekly (0.63 μmol m^{-2} s^{-1}) and then daily (0.97 μmol m^{-2} s^{-1}) models (Tables 1; S9). For CH_4 fluxes, the best-fitting ARIMA model was also identified at the monthly timescale (RMSE=0.41 μmol m^{-2} s^{-1}), with descending RMSE for the weekly and daily models ranging from 0.64 and 1.02 μmol m^{-2} $s^{-1,}$ respectively (Tables 1, S8). Full ARIMA results are reported in Table S9.

Table 1. *Best-fit results from Autoregressive Integrated Moving Average (ARIMA) analysis*

GHG	Timescale	Model Order	Surface Temp (°C)	DO Sat. (%)	Chl-a (µg L^{-1})	fDOM (RFU)	Inflow (m^3 s^{-1})	Thermo. Depth (m)	RMSE (µmol m^2 s^{-1})
CO2	Daily	(1,0,0)	0.18	-	-0.17	0.07	0.08	-0.09	0.97
	Weekly	(0,0,0)	0.64	-0.16	-	0.13	0.20	-0.19	0.63
	Monthly	(0,0,0)	0.73	-	-	0.24	-	-0.31	0.48
CH4	Daily	(0,0,0)	0.27	-	-	0.12	-	0.25	1.02
	Weekly	(0,1,1)	0.36	-	-	0.23	-0.36	0.24	0.64
	Monthly	(0,0,1)	0.74	-	-	-	-0.26	0.21	0.41

Note: Table includes only the top selected model (lowest corrected Akaike Information Criterion, AICc). Models are separated by greenhouse gas (GHG) flux as carbon dioxide (CO_2) and methane (CH_4) fluxes as well as by timescale (daily, weekly, monthly). Environmental predictors included: Surface temperature (Surface Temp, °C), dissolved oxygen saturation (DO Sat, %), Chlorophyll-*a* (Chl-*a*, µg L^{-1}), fluorescent dissolved organic matter (fDOM, RFU), inflow discharge (Inflow, m^3 s^{-1}), and thermocline depth (Thermo. Depth, m). Model order is specified as (p,d,q) where p is the order of the AR term, d is the order of the integration term, and q is the order of the MA term. For brevity, the autoregressive (AR) and moving average (MA) terms have been removed but can be found in the supplemental information. Results for all models with 2 AICc of the best fitting model, can be found in the supplemental information (Table S9). Dashed lines indicate environmental parameters that were not identified as statistically significant. The root mean square error (RMSE) is reported for each model. Standard errors for each parameter value are given in Table S9.

3.4 Influence of ice cover on CO_2 and CH_4 fluxes

FCR experienced two distinct winter regimes in 2021 vs. 2022. In 2021, ice-on first occurred on 10 January 2021, then came on and off multiple times before final ice-off on 23 February 2021. Overall, there were 27 days with some ice and 9 days with some open-water during the 2021 intermittent ice-period. In contrast, in 2022, there was a brief period of ice cover from 11 January to 14 January 2022, followed by continuous ice-on occurring from 16 January 2022 to final ice-off on 10 February 2022. While we were unable to collect ice thickness data through both winters due to safety concerns, peak ice thickness in FCR in 2022 was ~9.5 cm whereas peak ice thickness in 2021 was ~2 cm.

When comparing measured half-hourly fluxes aggregated across the intermittent ice-on period in winter 2021 and the continuous ice-on period in winter 2022, there were statistically-significantly higher median CO_2 and CH_4 fluxes measured during intermittent ice-on than continuous ice-on (Kruskal-Wallis $p<0.0001$; Fig. 5; Table S10). During intermittent ice-on in winter 2021, median CO_2 fluxes were 0.71 μmol m^{-2} s^{-1}, 2.5× higher than the median of 0.28 μmol m^{-2} s^{-1} during continuous ice-on in 2022. For CH_4, median fluxes were 0.001 μmol m^{-2} s^{-1} and -0.001 μmol m^{-2} s^{-1}, during intermittent ice-on and continuous ice-on, respectively (Table S10). Throughout the winter period, mean daily CO_2 and CH_4 fluxes were much lower and less variable than in the summer, for both years (Fig. 2, 3).

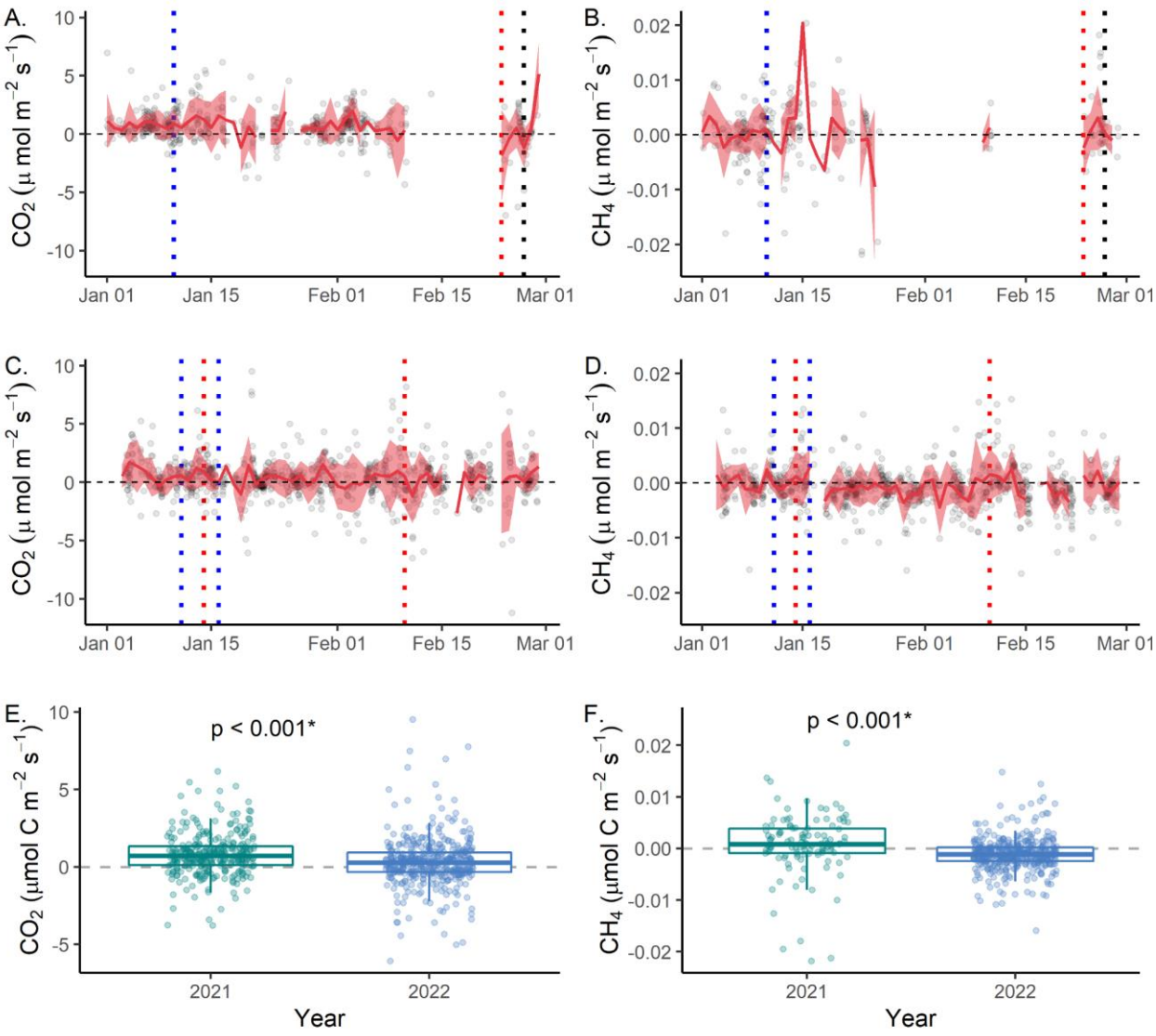

557

558 **Figure 5.** Mean daily fluxes during the winter of 2021 for A. Carbon dioxide (CO_2, µmol m^{-2} s^{-1})
559 and B. Methane (CH_4 µmol m^{-2} s^{-1}) during intermittent ice-on. Mean daily fluxes during winter
560 of 2022 for C. CO_2 and D. CH_4 during near-continuous ice-on. Grey dots represent measured
561 half-hourly fluxes while the solid red line indicates mean daily fluxes. The shaded red area
562 corresponds to the standard deviation (±1 S.D.) of the daily mean fluxes. The blue vertical
563 dashed lines correspond to the start of either intermittent or near-continuous ice-on for winter
564 2021 and 2022, respectively, while the red vertical dashed lines correspond to the start of
565 complete ice-off. The black dashed line in 2021 corresponds to spring mixing (first day after ice-
566 off when the temperature at 1 m and 8 m was < 1°C). For 2022, spring mixing was on the same
567 day as ice-off. Boxplots of measured E. CO_2 and F. CH_4 fluxes during each winter's intermittent
568 or continuous ice-on, respectively. For each box plot, the median is represented as the bold line
569 while the 25th and 75th percentiles are represented as the bottom and top of the box, respectively.
570 The whiskers represent minimum and maximum values (1.5× interquartile range). Points
571 represent all half hourly fluxes measured during the respective winter intermittent or continuous
572 ice-on, respectively period. The dashed horizontal line corresponds to zero fluxes. Asterisks

indicate statistically significant differences between median half-hourly fluxes measured during intermittent (2021) and continuous (2022) ice-on periods using Mann-Whitney-Wilcoxon tests ($\alpha = 0.05$).

3.5 Net CO_2 and CH_4 balance for a small, eutrophic reservoir

Gap-filled CO_2 and CH_4 half-hourly fluxes summed across the entire year indicate that FCR was an overall source of CO_2 and CH_4 to the atmosphere (Fig. 6). According to gap-filled EC fluxes, FCR released 633 and 731 g CO_2-C m^{-2} $year^{-1}$, during the first and second years of the study, respectively. For gap-filled CH_4 fluxes, FCR released 1.02 and 1.29 g CH_4-C m^{-2} $year^{-1}$, respectively. Although substantial gap-filling was needed, the gap-filled and measured data yielded similar estimates when the measured data were scaled by the percentage of missing data from the measured time series (Fig. S12).

The annual GHG balances were driven by large fluxes of CO_2 and CH_4 during the summer. Net emissions during the warmest months (June – September; 375 and 496 g CO_2-C m^{-2} for year 1 and year 2, respectively) represented up to 68% of the total annual net CO_2 flux as compared to the coldest months (December – March) when only 98 and 57 g CO_2-C m^{-2} was emitted (up to 15% of the total annual CO_2). Similarly, for CH_4, up to 66% of the total annual net CH_4 flux was released during the warmest months (June – September; 0.67 and 0.76 g CH_4-C m^{-2}) and less than 1% during the coldest months (December – March). For the second year of monitoring, annual fluxes were greater for both CO_2 and CH_4, largely due to elevated fluxes in early and late fall (September – November). Cumulatively, the amount of CO_2-C released from FCR was three orders of magnitude greater than the mass of CH_4-C released.

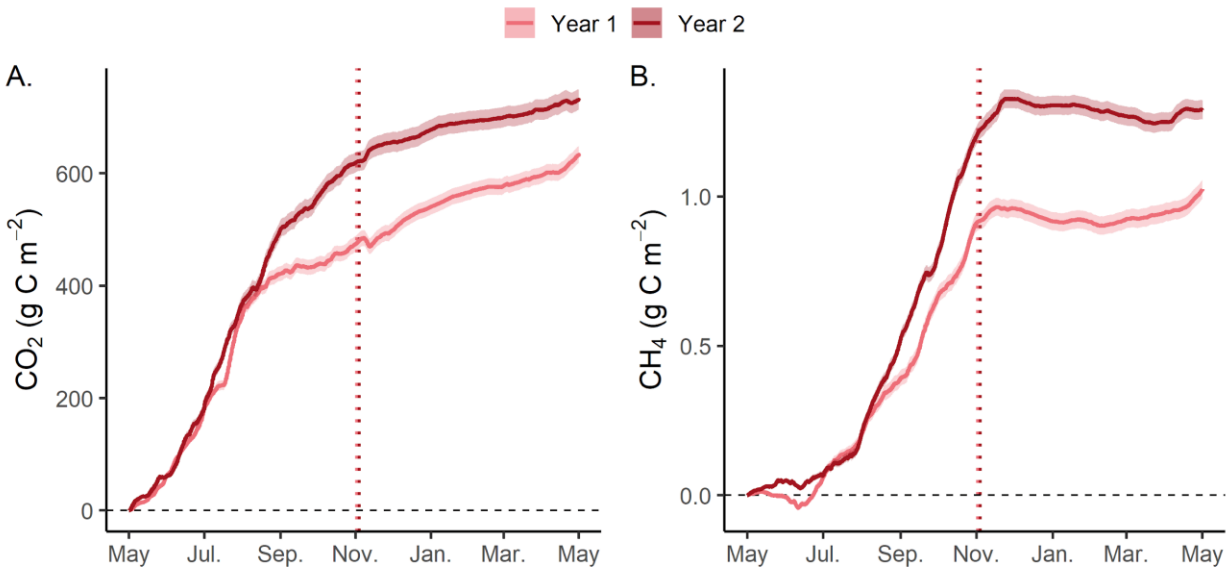

Figure 6. Annual cumulative fluxes using measured and gap-filled eddy covariance (EC) data for A. carbon dioxide (CO_2, g C m^{-2}) and B. methane (CH_4, g C m^{-2}) from Falling Creek Reservoir for Year 1 (May 2020-April 2021; pink) and Year 2 (May 2021-April 2022; dark red). Shaded areas correspond to the aggregated standard deviation (±1 S.D.) of measurements. The horizontal dashed line corresponds to zero and the vertical dotted line indicates reservoir fall turnover for both years.

4 Discussion

This study provides the first annual-scale, multi-year estimates of *both* CH_4 and CO_2 fluxes using an EC system from a small reservoir. While using EC systems in small freshwaters is inherently challenging and contains several limitations, our work reveals variable patterns in both CO_2 and CH_4 fluxes over sub-daily to seasonal scales that set the stage for future work. Our study was limited by low levels of measured data, underscoring the need for more accurately quantifying the GHG contributions of small reservoirs on multiple timescales. Despite these challenges, however, our data suggest that FCR was a substantial CO_2 and CH_4 source to the atmosphere on multiple timescales. Below we discuss some of the challenges of using an EC system in small freshwaters as well as the patterns and potential drivers of variability in fluxes (CO_2 and CH_4) over multiple timescales, including during winter ice-cover.

4.1 Variability in sub-daily fluxes, with higher dawn than dusk CO_2 fluxes

A key advantage of an EC system is the ability to capture variability in sub-daily GHG fluxes throughout the year. Despite data gaps and limitations, the fluxes collected by the EC represent a substantial increase in the ability to identify variability in GHG fluxes at multiple timescales. Our work complements previous studies of freshwater systems using EC measurements that observed high sub-daily variability in both summer CO_2 (Liu et al. 2016; Golub et al. 2021; Shao et al. 2015) and CH_4 fluxes (Eugster et al. 2011; Podgrajsek et al. 2014; Taoka et al. 2020; Waldo et al. 2021) and furthers our understanding of the variability of CO_2 and CH_4 fluxes on multiple timescales.

When comparing day (11:00 to 13:00) versus night (23:00 to 01:00) fluxes, we observed no statistically significant differences between CO_2 or CH_4 fluxes using measured EC fluxes aggregated over the two-year monitoring period (Fig. 4; Table S6). When repeating this analysis separately among seasons, we did observe a statistically significant difference between day and night for CH_4 fluxes during the winter, but that was the only season where statistical differences were detected (Table S11). Similarly, studies in a small Finnish lake also found no evidence for diel differences in CO_2 fluxes (Erkkiliä et al. 2018; Mammarella et al. 2015), while Waldo et al. (2021) found diel differences in CH_4 fluxes on only 18.5% of days out of a 2-year study period. Other studies, however, have observed more consistent diel patterns in GHG fluxes. For example, some studies have shown higher CH_4 fluxes during the night in lakes and reservoirs (Eugster et al. 2011; Podgrasjek et al. 2014; Waldo et al. 2021) and higher CO_2 fluxes at night in streams (Attermeyer et al. 2021; Gómez-Gener et al. 2021). On the other hand, some studies observed higher CH_4 fluxes during the day as compared to night (Erkkiliä et al. 2018; Jammet et al. 2017; Podgrasjek et al. 2016; Sieczko, et al. 2020). Our results are contrary to our predictions, in which we expected statistically higher CO_2 fluxes during the day due to significantly higher wind speeds. We hypothesize that higher concentrations of dissolved CO_2 in the surface waters at night, due to decreased primary productivity and elevated microbial respiration or convective mixing of deeper waters with higher dissolved GHG concentrations (Liu et al. 2016; Fig. S13), were not efficiently transferred to the atmosphere at the low observed nightly wind speeds, resulting in similar flux magnitudes during both day and night. Clearly, there is a range of responses to diel variation among lake and reservoir CO_2 and CH_4 fluxes, and more work is

needed to identify when, where, and why lakes and reservoirs may emit differential GHGs during day vs. night.

While we did not observe statistically significant differences between GHG fluxes measured during the day as compared to night, we did observe statistically significantly higher CO_2 fluxes at dawn (05:00 to 07:00) as compared to dusk (17:00 to 19:00), but no difference in dawn vs. dusk CH_4 fluxes over the full study period (Fig. 4). Similarly, studies conducted in other lakes also found CO_2 flux minima during the late afternoon (~18:00) and CO_2 flux maxima during the early morning (~06:00; Liu et al. 2016; Shao et al. 2015), supporting our observations of higher dawn CO_2 fluxes. Liu et al. (2016) hypothesized the lower CO_2 fluxes observed during the day (~18:00) were likely a result of elevated primary productivity during the afternoon, primarily in the summer months, but could have also been due to convective mixing in the water column at night.

Altogether, our results provide additional evidence that the time of sample collection has important implications for upscaling freshwater GHG fluxes to longer timescales (Attermeyer et al. 2021; Gómez-Gener et al. 2021). A previous study conducted in FCR which estimated CO_2 and CH_4 diffusive fluxes using discrete GHG measurements collected at ~noon concluded FCR was often a small CO_2 sink during the summer stratified period in 2015-2016 (McClure et al. 2018), whereas our diel EC data indicate that FCR was an overall CO_2 source throughout the summer in both 2020 and 2021. While the flux magnitudes measured by McClure et al. (2018) were similar to the present study, the overall conclusions were different due to the temporal resolution of sample collection.

4.2 Important role of water temperature and thermocline depth in constraining daily, weekly, and monthly CO_2 and CH_4 fluxes

Following our analysis of CO_2 and CH_4 fluxes over daily to seasonal timescales, we then used time-series analysis to test the potential effects of various limnological variables on GHG fluxes. Specifically, ARIMA results show that surface water temperature was positively correlated with both CO_2 and CH_4 fluxes at the daily, weekly, and monthly timescales (Table 1). These results were supported by higher fluxes of both CO_2 and CH_4 observed during the warmer summer months when aggregated to daily, weekly, and monthly timescales (Fig. 2, 3, S8).

Strong positive correlations between GHG fluxes (both CO_2 and CH_4) and water temperature have been observed in several freshwater ecosystems, especially on longer timescales, with clear differences between summer and winter fluxes (monthly to seasonally; Eugster et al. 2011; Reed et al. 2018; Taoka et al. 2020). Higher GHG fluxes were expected during the summer as compared to winter, due to elevated rates of biological respiration stimulated by higher temperatures in both the surface and deep waters (Fig. S13). Generally, water column dissolved GHG concentrations increased throughout the summer period (Fig. S13). In the surface waters, dissolved CH_4 concentrations generally peaked in July, while dissolved CO_2 concentrations increased throughout the summer and peaked around fall turnover.

In addition to temperature, thermocline depth was also identified as an important environmental parameter controlling both CO_2 and CH_4 fluxes. For CO_2 fluxes, thermocline depth was negatively associated with fluxes at all timescales, indicating higher CO_2 fluxes when the thermocline was shallower. Generally, thermocline depth was shallower in the late summer (Fig. S7) when CO_2 fluxes were observed to be greatest and most variable in FCR. This pattern may be indirectly related to water temperature, as shallower thermocline depths were weakly, negatively associated with warmer water temperatures, and there was a strong positive relationship between CO_2 fluxes and water temperature, as discussed above.

Conversely, thermocline depth was positively correlated with CH_4 fluxes at all timescales (daily, weekly, monthly), indicating higher CH_4 fluxes when the thermocline depth was deeper, which was generally observed during the late summer and early fall as mixing increased (Fig. S7). Previous studies have suggested water column mixing is an important control on CH_4 fluxes, leading to higher fluxes during convective and wind-driven mixing when high dissolved concentrations of CH_4 accumulated in the deeper waters are mixed to the surface, which would be more common when the thermocline depth is deeper (Sieczko et al. 2021). We did observe elevated dissolved CH_4 concentrations in the metalimnion (3.8 - 5 m), particularly in the late summer and early fall when the thermocline started to deepen (Fig. S7, S13), which was likely mixed into the surface waters and contributed to reservoir CH_4 fluxes, as observed previously in FCR by McClure et al. (2018). However, we do not know the extent of methanotrophy in converting dissolved CH_4 to CO_2 prior to emissions. While we also observed elevated dissolved CO_2 concentrations at similar depths during the late summer and early fall, we might expect

elevated primary production observed at this same time (Fig. S6) reduced overall fluxes of CO_2 from the reservoir. Additional research is needed to specifically link water column dissolved GHG concentrations and water column processes with atmospheric emissions.

Following temperature and thermocline depth, fDOM was identified as a key positive environmental predictor for CO_2 fluxes at all timescales (daily, weekly, monthly; Table 1). A similar positive relationship between terrestrially-derived DOM and dissolved CO_2 was identified in 48 Canadian streams (D'Amario and Xenopoulos, 2015). As fDOM sensors are thought to mainly capture allochthonous DOM (Howard et al. 2021; Watras et al. 2015), this finding suggests that allochthonous DOM from the reservoir's primary inflow stream or diffuse overland flow may result in elevated CO_2 emissions from freshwater ecosystems as allochthonous DOM is converted to CO_2 during respiration. This follows previous research which has identified allochthonous carbon inputs and associated DOC concentrations as important predictors of CO_2 fluxes in lakes and reservoirs (Barros et al. 2011; Sobek et al. 2005). Unlike for CO_2, fDOM was only identified as an important environmental predictor for CH_4 fluxes at shorter timescales (daily, weekly). In an analysis of >300 lakes, Sanches et al. (2019) found a strong positive relationship between dissolved organic C and diffusive CH_4 fluxes, suggesting dissolved organic C availability for methanogenesis may play an important role in constraining CH_4 fluxes across multiple lakes and timescales. The strong positive correlation between CH_4 fluxes and fDOM observed here further indicates that dissolved organic C, as a proxy from fDOM (Howard et al. 2021), may also be important at the local scale on short-timescales.

In addition to these overarching patterns, several environmental parameters were intermittently important for various timescales for either CO_2 or CH_4 fluxes. CO_2 fluxes were positively correlated with inflow at shorter timescales (daily, weekly) while CH_4 fluxes were negatively correlated with inflow but only at longer timescales (weekly, monthly; Table 1). Following the positive relationship between CO_2 fluxes and fDOM, we hypothesize the positive relationship with inflow reflects the importance of allochthonous DOM delivery to FCR via the primary inflow and diffuse overland flow, which suggests a potentially labile source of allochthonous DOM to the reservoir via the primary inflow. Pearson correlation analysis, suggests fDOM and inflow were weakly correlated at these timescales (daily, weekly; $\rho = 0.13$,

0.11, respectively), but was weakly negatively correlated at longer timescales (monthly, ρ = -0.03; Table S4). Previous research examining CH_4 fluxes from FCR have found similar negative relationships between inflow and CH_4 fluxes, especially via ebullition in the upstream, littoral portion of the reservoir (McClure et al. 2020). Results from this study suggest inflow is similarly correlated with CH_4 fluxes at the deepest point of the reservoir, primarily on longer timescales (weekly, monthly). Finally, Chl-a was negatively associated with CO_2 fluxes at the daily timescale while DO sat. was negatively associated with CO_2 fluxes at the weekly timescale (Table 1). Both of these relationships suggest a coupling between high primary production, as indicated by high Chl-a and high DO Sat., and low CO_2 fluxes on shorter timescales (daily, weekly). Previous studies have identified a weak negative relationship between primary production and CO_2 fluxes on the sub-daily timescale in other eutrophic, freshwater lakes and reservoirs (Liu et al. 2016; Shao et al. 2015).

4.3 Role of fall turnover and ice cover in affecting GHG dynamics

Contrary to previous studies conducted in both FCR and other thermally-stratified waterbodies (e.g., Erkkiliä et al. 2018; McClure et al. 2018; 2020), we observed low CO_2 and CH_4 fluxes during the days surrounding fall turnover for both years (1 November 2020; 3 November 2021), when EC data indicate that FCR was a small to negligible CO_2 and CH_4 source (Fig. 2, 3, S9). Discrete diffusive fluxes measured on the day of fall turnover suggest FCR was a 4x and 14x larger CO_2 source than fluxes measured with the EC, in years 1 and 2 respectively (Figs. 2, S9). Similar to CO_2, we found the magnitude of CH_4 fluxes decreased following fall turnover but remained a small source (Fig. 3, S9). McClure et al. (2018) observed episodic release of CH_4 from FCR during the weeks prior to fall turnover as high concentrations of dissolved CH_4 that had accumulated in the middle of the water column, due to the formation of a metalimnetic oxygen minimum, were emitted during wind-mixing. In the weeks prior to fall turnover, we did observe elevated CH_4 emissions in both years (Figs. 3, S9), supporting this observed mechanism (McClure et al. 2018; Fig. S13), and decreasing the importance of fall turnover as a single pulse of emissions. For CO_2, similar increases in dissolved CO_2 concentrations were observed in the metalimnion during the same time period, but as suggested above, the release of this CO_2 to the atmosphere was likely mitigated by primary production in the surface waters.

Importantly, this study provides some of the first near-continuous flux measurements of *both* CO_2 and CH_4 during winter, including during intermittent and continuous ice-on conditions (Fig. 5). Overall, the annual GHG balance was driven by large fluxes of CO_2 and CH_4 during the summer, as CO_2 and CH_4 fluxes were 3× and 23× greater, respectively, during the summer stratified period (April – October) as compared to the winter and early spring (November – March; Fig. 6). However, we do note that we observed significantly higher CO_2 and CH_4 fluxes during intermittent ice-on when there is likely more air-water gas exchange as compared to continuous ice-on ($p<0.001$; Fig. 5; Table S10), which would physically limit air-water gas exchange, thereby demonstrating the importance of annually-variable, winter ice dynamics to seasonal GHG fluxes. Of the studies that report GHG fluxes during continuous ice-on, all report low fluxes with low variability (A.K. Baldocchi et al. 2020; Jammet et al. 2015, 2017; Reed et al. 2018), similar to the winter with continuous ice-on at FCR. Interestingly, these studies also noted high fluxes immediately following ice-off for both CO_2 and CH_4 due to accumulation of dissolved CO_2 and CH_4 under the ice from aerobic and anaerobic microbial respiration (Anderson et al. 1999; A.K. Baldocchi et al. 2020; Gorsky et al. 2021; Jammet et al. 2015, 2017; Podgrajsek et al. 2015; Takoa et al. 2020), which was not observed at FCR. Unlike these previous studies, which were largely conducted in northern lakes which are frozen for months at a time, FCR is a more temperate system which only periodically freezes for a few days to weeks at time (Carey and Breef-Pilz, 2022). We hypothesize that the brief continuous ice-cover observed at FCR during winter 2022 (25 days) was not long enough to promote extensive accumulation of dissolved GHGs under ice, as observed by the other studies. Further work on the effect of ice cover on GHG fluxes is needed, but our comparison of intermittent ice-on vs. continuous ice-on suggests that the increasing intermittent ice-cover being experienced in many lakes worldwide (Imrit and Sharma, 2021; Sharma et al. 2021; Woolway et al. 2020) will likely increase winter GHG fluxes. These increases may be due to both greater continuous exchange of GHGs across the air-water interface and increased rates of microbial respiration under higher winter temperatures.

4.4 Much higher annual CO_2 emissions from FCR than other studied reservoirs

When scaling fluxes to the full year, FCR was a much smaller annual CH_4 source (1.02-1.29 g m^{-2} yr^{-1}), yet a larger CO_2 source (633-731 g m^{-2} yr^{-1}; Figs. 5, S12), than other reservoirs

reported in the literature to date (A.K. Baldocchi et al. 2020; Deemer et al. 2016; Golub et al. 2021). While the total magnitude of CO_2 emissions from FCR was greater than most studies, Golub et al. (2021) similarly found that data from 12 lakes and reservoirs over multiple years emitted substantial amounts of CO_2 in their synthesis of EC measured CO_2 fluxes in freshwaters (13.6 - 224 g C m^{-2} yr^{-1}), except for one reservoir during one year which had a CO_2 flux of -53.6 g C m^{-2} yr^{-1}. As compared to other reservoirs with GHG flux data, FCR is old (>100 years old) which may lead to lower GHG emissions, particularly for CH_4 fluxes, likely as a result of reduced supply of organic matter substrate in the sediments as the reservoir ages (Barros et al. 2011; McClure et al. 2020; Prairie et al. 2018).

Despite its age, however, FCR was a much larger CO_2 source as compared to other lakes and reservoirs. The CO_2 emissions were consistently high among years, suggesting that FCR may be a greater source of CO_2 than most terrestrial environments (-750 to 250 g C m^{-2} yr^{-1} for multi-year, undisturbed terrestrial sites; D.D. Baldocchi et al. 2020). Comparisons between years suggest that slightly higher annual fluxes of CO_2 and CH_4 in the early to late fall (September - November) of the first monitoring year as compared to the second year may be related to slightly higher mean air temperatures or lower inflow levels (and corresponding longer hydraulic residence times), though this remains unknown. We note that these cumulative fluxes are likely conservative, as there were substantial gaps in measured EC fluxes during year 1, particularly in August 2020, likely resulting in underestimated measured fluxes during this time of year when fluxes are usually highest (Fig. 6, S12). Multiple meteorological, biological, and environmental processes likely contributed to the higher observed annual CO_2 fluxes as compared to other lakes and reservoirs. Additional studies comparing GHG fluxes from multiple reservoirs simultaneously are needed to identify these variables.

4.5 Challenges of using EC systems in small, freshwater lakes and reservoirs

While the study described here greatly expands the temporal frequency of measured CO_2 and CH_4 fluxes from a small reservoir, several caveats must be taken into consideration. EC systems are notoriously difficult to use in freshwater ecosystems due to footprint considerations (Vesala et al. 2006), frequent occurrences of low u* values, particularly at night (Vesala et al. 2006; Scholz et al. 2021), as well as general considerations resulting in high percentages of data

removed due to these and other issues (yielding data coverage of 10 – 40%; e.g., A.K. Baldocchi et al. 2020; Erkkiliä et al. 2018; Huotari et al. 2011; Ouyang et al. 2017; Shao et al. 2015; Waldo et al. 2021; Table S1). While low data coverage was common in the current study, data gaps were relatively consistent across timescales (daily to seasonally) to ensure unbiased data. Furthermore, compared to the temporal frequency of many grab sample methods (i.e., samples measured weekly, biweekly, or monthly), the data coverage of the EC system is still a substantial improvement and more accurately captures fluxes across multiple timescales challenging to sample, such as at night, during winter ice-cover, and during episodic events, such as fall turnover. Importantly, we note that standard gap-filling routines for EC flux data collected from freshwater ecosystems (i.e., lakes and reservoirs) do not currently exist. We applied gap-filling routines originally developed for terrestrial ecosystems (Wutzler et al. 2018) to FCR to better estimate annual scale fluxes, which is still a substantial improvement over traditional grab sampling methods.

While strict filtering processes were enacted to limit non-local fluxes (i.e., filtering fluxes when the along-wind distance providing 90% of the cumulative contribution was outside the reservoir), we are unable to completely rule out potential non-local processes (e.g., land-lake interactions) which occur outside the footprint and are entrained or advected into the EC footprint area (Esters et al. 2020; Vesala et al. 2006, 2011; Fig. S2). These processes may be particularly important in small freshwaters located in mountainous regions (Scholz et al. 2021). For example, Scholz et al. (2021) found reduced nighttime CO_2 emissions due to low wind speeds and CO_2 sinking from the land to the lake surface at night in a mountainous Swiss lake. While the topography at FCR is not as extreme, similar processes may be occurring at FCR, though at a smaller scale. In addition, based on studies conducted in similar terrestrial ecosystems, we might expect negative CO_2 fluxes in the summer followed by substantial CO_2 emissions in the fall and winter; however, these patterns were not observed in FCR, suggesting the majority of fluxes measured in this study likely originated in the reservoir. When considered and interpreted cautiously, the data collected by the EC system provides a far more comprehensive time series than what is possible from discrete measurements (Anderson et al. 1999; Eugster 2003; Houtari et al. 2011; Jonsson et al. 2008; Scholz et al. 2021), which is critical for increasing our understanding of GHG fluxes from small reservoirs on multiple temporal scales.

Finally, comparisons with diffusive grab samples suggest fluxes measured with the EC system were consistently higher than those estimated with diffusive grab samples, especially for CO_2 (Fig 2, S11), which is consistent with previous studies (Scholz et al. 2021, and references therein). Conversely, CH_4 fluxes calculated using the discrete diffusive methods were more comparable to those measured by the EC system (Fig. 3, S11). Discrepancies between EC measured fluxes and diffusive grab samples may be a result of the different spatial resolution of the two methods, where the EC system is measuring fluxes both at the deepest point of the reservoir in addition to upstream and littoral portions of the reservoir while diffusive grab samples were only collected at the deepest point of the reservoir (Fig. 1; Scholz et al. 2021). Indeed, several studies have observed higher CO_2 and CH_4 fluxes in the littoral zone, closer to the shore, which would have been encompassed in the measured EC fluxes but not the diffusive grab samples (Erkkiliä et al. 2018; Scholz et al. 2021; Taoka et al. 2020). A comparison of CH_4 fluxes on an inflow to dam transect at FCR observed substantially higher fluxes in the littoral zone, supporting this pattern (McClure et al. 2020).

5 Conclusions

Overall, we observed FCR to be a source of CO_2 and CH_4 to the atmosphere on annual timescales. Given the limitations of gap-filling, our calculated annual fluxes (~633-731 g CO_2-C m^{-2} yr^{-1}; ~1.02-1.29 g CH_4-C m^{-2} yr^{-1}) are only estimates, however, we note their remarkable consistency between years. Importantly, by measuring fluxes near-continuously for a full year, we found winter fluxes (December-March) of both CO_2 and CH_4 to be comparatively smaller (15-25% and <1% of total annual fluxes, respectively) than the summer stratified period (June - September) yet still important for annual GHG fluxes. In addition, measuring GHG fluxes during two winters with contrasting ice-cover, showed significantly higher CO_2 and CH_4 fluxes during intermittent as compared to continuous ice-on. Finally, we identified surface water temperature, thermocline depth, and several other environmental variables (fDOM, inflow) as important drivers of both CO_2 and CH_4 fluxes on multiple timescales. Altogether, our results suggest that CO_2 and CH_4 are highly dynamic on multiple temporal scales and highlight the role of small reservoirs as important GHG sources in global budgets. Ultimately, efforts to scale up small reservoir CO_2 and CH_4 emissions will need to consider how the environmental processes that

drive C dynamics in small reservoirs may differ from larger waterbodies, which in turn could alter reservoir fluxes. Given the ubiquity of small (<1 km^2) reservoirs in the landscape, quantifying their contributions to the global C cycle is paramount, especially given that our study suggests that they may emit more CO_2 and CH_4 than would be expected from their surface area.

Acknowledgments

This project originated in February 2020 and was made possible through creative teamwork spanning international borders amidst a global pandemic. We thank Bobbie Niederlehner, Bethany Bookout, Heather Wander, Abigail Lewis, Whitney Woelmer, Dexter Howard, Nicholas Hammond, Arpita Das, Ryan McClure, Mary Lofton, and Calvin Thomas for their assistance with field collection and laboratory analysis. Zoran Nesic and Vahid Daneshmand provided critical troubleshooting assistance and technical support. Additionally, we thank the Western Virginia Water Authority (WVWA), especially Jamie Morris, for long-term access to field sites and logistical support. We gratefully acknowledge funding from U.S. National Science Foundation grants CNS-1737424, DEB-1753639, DEB-1926050, DBI-1933102, and DBI-1933016; and Fralin Life Sciences Institute at Virginia Tech. We also acknowledge Discovery Grant support to Johnson provided by the Natural Sciences and Engineering Research Council of Canada (NSERC), RGPIN-2020-06252. The authors report no conflicts of interest.

Open Research

The eddy covariance dataset and associated QA/QC code for this study can be found in the Environmental Data Initiative (EDI) repository via https://doi.org/10.6073/pasta/a1324bcf3e1415268996ba867c636489 and https://portal-s.edirepository.org/nis/mapbrowse?packageid=edi.920.2 (Carey et al. 2022a). Additionally, code used for the timeseries and ARIMA analyses are archived at https://10.5281/zenodo.742001 (Zenodo; Hounshell et al. 2022). Additional datasets including the meteorological data set (https://portal-s.edirepository.org/nis/mapbrowse?packageid=edi.143.17, Carey et al. 2022c), limnological dataset (https://doi.org/10.6073/pasta/81c6c76f4fe22434a20aa8c00f2d4ad1 and

https://portal-s.edirepository.org/nis/mapbrowse?packageid=edi.518.11, Carey et al. 2022d), inflow discharge (https://doi.org/10.6073/pasta/c65755d4c0102dde6e3140c1c91b77d6 and https://portal-s.edirepository.org/nis/mapbrowse?packageid=edi.923.1, Carey et al. 2022e), ice-cover (https://portal.edirepository.org/nis/mapbrowse?packageid=edi.456.4, Carey and Breef-Pilz, 2022), and dissolved discrete grab greenhouse gas concentrations (https://doi.org/10.6073/pasta/2fb836492aace4c13b7962f2718be8e5 and https://portal-s.edirepository.org/nis/mapbrowse?scope=edi&identifier=928&revision=3, Carey et al. 2022b) are also archived in the EDI. All data (2020-2022) are available for review in the EDI staging environment and will be published following manuscript acceptance. All data through 2021 have been published to EDI and are available under the Creative Commons License - Attribution.

References

Anderson, D.E., Striegl, R.G., Stannard, D.I., Michmerhuizen, C.M., McConnaughey, T.A., & LaBaugh, J.W. (1999). Estimating lake-atmosphere CO_2 exchange. *Limnology and Oceanography*, *44*(4), 988–1001. https://doi.org/10.4319/lo.1999.44.4.0988

Attermeyer, K., Casas-Ruiz, J.P., Fuss, T., Pastor, A., Cauvy-Fraunié, S., Sheath, D., et. al. (2021). Carbon dioxide fluxes increase from day to night across European streams. *Communications Earth & Environment*, *2*(1), 118. https://doi.org/10.1038/s43247-021-00192-w

Baldocchi, A.K., Reed, D.E., Loken, L.C., Stanley, E.H., Huerd, H., & Desai, A.R. (2020). Comparing spatial and temporal variation in lake-atmosphere carbon dioxide fluxes using multiple methods. *Journal of Geophysical Research: Biogeosciences, 125*(12). https://doi.org/10.1029/2019JG005623

Baldocchi, D.D. (2020). How eddy covariance flux measurements have contributed to our understanding of Global Change Biology. *Global Change Biology*, *26*(1), 242–260. https://doi.org/10.1111/gcb.14807

Barros, N., Cole, J.J., Tranvik, L.J., Prairie, Y.T., Bastviken, D., Huszar, V.L.M., del Giorgio, P., & Roland, F. (2011). Carbon emission from hydroelectric reservoirs linked to reservoir age and latitude. *Nature Geoscience*, *4*(9), 593–596. https://doi.org/10.1038/ngeo1211

Bartosiewicz, M., Przytulska, A., Lapierre, J., Laurion, I., Lehmann, M.F., & Maranger, R. (2019). Hot tops, cold bottoms: Synergistic climate warming and shielding effects increase carbon burial in lakes. *Limnology and Oceanography Letters*, *4*(5), 132–144. https://doi.org/10.1002/lol2.10117

Bastviken, D., Sundgren, I., Natchimuthu, S., Reyier, H., & Gålfalk, M. (2015). Technical Note: Cost-efficient approaches to measure carbon dioxide (CO_2) fluxes and concentrations in terrestrial and aquatic environments using mini loggers. *Biogeosciences*, *12*(12), 3849–3859. https://doi.org/10.5194/bg-12-3849-2015

946 Bastviken, D., Tranvik, L.J., Downing, J.A., Crill, P.M., & Enrich-Prast, A. (2011). Freshwater
947 Methane Emissions Offset the Continental Carbon Sink. *Science*, *331*(6013), 50–50.
948 https://doi.org/10.1126/science.1196808

949 Beaulieu, J.J., DelSontro, T., & Downing, J.A. (2019). Eutrophication will increase methane
950 emissions from lakes and impoundments during the 21st century. *Nature*
951 *Communications*, *10*(1), 1375. https://doi.org/10.1038/s41467-019-09100-5

952 Burba, G., & Anderson, D. (2010). A brief practical guide to eddy covariance flux
953 measurements: principles and workflow examples for scientific and industrial
954 applications. Li-Cor Biosciences. Chicago.
955 https://www.licor.com/env/pdf/eddy_covariance/Brief_Intro_Eddy_Covariance.pdf

956 Burba, G., Schmidt, A., Scott R.L., Nakai, T., Kathilankal, J., Fratini, G., et al. (2012).
957 Calculating CO_2 and H_2O eddy covariance fluxes from an enclosed gas analyzer using an
958 instantaneous mixing ratio. Global Change Biology, *18*(1), 385-399.
959 https://doi.org/10.1111/j.1365-2486.2011.02536.x

960 Burnham, K.P., & Anderson, D.R. (2002). *Model selection and multimodel inference: a practical*
961 *information-theoretic approach*. New York, NY: Springer.

962 Butman, D., Stackpoole, S., Stets, E., McDonald, C.P., Clow, D.W., & Striegl, R.G. (2016).
963 Aquatic carbon cycling in the conterminous United States and implications for terrestrial
964 carbon accounting. *Proceedings of the National Academy of Sciences*, *113*(1), 58–63.
965 https://doi.org/10.1073/pnas.1512651112

966 Carey, C.C. & Breef-Pliz, A. (2022). Ice cover data for Falling Creek Reservoir, Vinton,
967 Virginia, USA for 2013-2022. (Version 4). [Dataset]. Environmental Data Initiative
968 (EDI). https://portal.edirepository.org/nis/mapbrowse?packageid=edi.456.4

969 Carey, C.C., Breef-Pilz, A. & Bookout, B.J. (2022c). Time series of high-frequency
970 meteorological data at Falling Creek Reservoir, Virginia, USA 2015-2021 (Version 14).
971 [Dataset]. Environmental Data Initiative (EDI). https://portal-
972 s.edirepository.org/nis/mapbrowse?scope=edi&identifier=143&revision=14

Carey, C.C., Breef-Pilz, A., Hounshell, A.G., Lofton, M.E., McClure, R.P., Gerling, A.B., & Woelmer, W.M. (2022e). Discharge time series for the primary inflow tributary entering Falling Creek Reservoir, Vinton, Virginia, USA 2013-2021. (Version 8). [Dataset]. Environmental Data Initiative (EDI). https://doi.org/10.6073/pasta/c65755d4c0102dde6e3140c1c91b77d6

Carey, C.C., Breef-Pilz, A., Woelmer, W.M., & Bookout, B.J. (2022d). Time series of high-frequency sensor data measuring water temperature, dissolved oxygen, pressure, conductivity, specific conductance, total dissolved solids, chlorophyll a, phycocyanin, and fluorescent dissolved organic matter at discrete depths in Falling Creek Reservoir, Virginia, USA in 2018-2021. (Version 6). [Dataset]. Environmental Data Initiative (EDI). https://doi.org/10.6073/pasta/81c6c76f4fe22434a20aa8c00f2d4ad1

Carey, C.C., Hounshell, A.G., D'Acunha, B.M., Breef-Pilz, A., Thomas, R.Q., & Johnson, M.S. (2022a). Time series of carbon dioxide and methane fluxes measured with eddy covariance for Falling Creek Reservoir in southwestern Virginia, USA during 2020-2022. (Version 1). [Dataset]. Environmental Data Initiative (EDI). https://doi.org/10.6073/pasta/a1324bcf3e1415268996ba867c636489

Carey, C.C., Hounshell, A.G., McClure, R.P., Gerling, A.B., Lewis, A.S.L., & Niederlehner, B.R. (2022b). Time series of dissolved methane and carbon dioxide concentrations for Falling Creek Reservoir and Beaverdam Reservoir in southwestern Virginia, USA during 2015-2021. (Version 6). [Dataset]. Environmental Data Initiative (EDI). https://doi.org/10.6073/pasta/2fb836492aace4c13b7962f2718be8e5

Cole, J.J., & Caraco, N.F. (1998). Atmospheric exchange of carbon dioxide in a low-wind oligotrophic lake measured by the addition of SF_6. *Limnology and Oceanography*, *43*(4), 647–656. https://doi.org/10.4319/lo.1998.43.4.0647

Cole, J.J., Prairie, Y.T., Caraco, N.F., McDowell, W.H., Tranvik, L.J., Striegl, R.G., et. al. (2007). Plumbing the Global Carbon Cycle: Integrating Inland Waters into the Terrestrial Carbon Budget. *Ecosystems*, *10*(1), 172–185. https://doi.org/10.1007/s10021-006-9013-8

Crusius, J., & Wanninkhof, R. (2003). Gas transfer velocities measured at low wind speed over a lake. *Limnology and Oceanography*, *48*(3), 1010–1017. https://doi.org/10.4319/lo.2003.48.3.1010

D'Amario, S.C., & Xenopoulos, M.A. (2015). Linking dissolved carbon dioxide to dissolved organic matter quality in streams. *Biogeochemistry*, *126*(1–2), 99–114. https://doi.org/10.1007/s10533-015-0143-y

Deemer, B.R., Harrison, J.A., Li, S., Beaulieu, J.J., DelSontro, T., Barros, et. al. (2016). Greenhouse Gas Emissions from Reservoir Water Surfaces: A New Global Synthesis. *BioScience*, *66*(11), 949–964. https://doi.org/10.1093/biosci/biw117

Deemer, B.R., & Holgerson, M.A. (2021). Drivers of Methane Flux Differ Between Lakes and Reservoirs, Complicating Global Upscaling Efforts. *Journal of Geophysical Research: Biogeosciences*, *126*(4). https://doi.org/10.1029/2019JG005600

DelSontro, T., del Giorgio, P.A., & Prairie, Y.T. (2018). No Longer a Paradox: The Interaction Between Physical Transport and Biological Processes Explains the Spatial Distribution of Surface Water Methane Within and Across Lakes. *Ecosystems*, *21*(6), 1073–1087. https://doi.org/10.1007/s10021-017-0205-1

Erkkilä, K.M., Ojala, A., Bastviken, D., Biermann, T., Heiskanen, J.J., Lindroth, A., et. al. (2018). Methane and carbon dioxide fluxes over a lake: Comparison between eddy covariance, floating chambers and boundary layer method. *Biogeosciences*, *15*(2), 429–445. https://doi.org/10.5194/bg-15-429-2018

Esters, L., Rutgersson, A., Nilsson, E., & Sahlée, E. (2021). Non-local Impacts on Eddy-Covariance Air–Lake CO_2 Fluxes. *Boundary-Layer Meteorology*, *178*(2), 283–300. https://doi.org/10.1007/s10546-020-00565-2

Eugster, W. (2003). CO_2 exchange between air and water in an Arctic Alaskan and midlatitude Swiss lake: Importance of convective mixing. *Journal of Geophysical Research*, *108*(D12), 4362. https://doi.org/10.1029/2002JD002653

Eugster, W., DelSontro, T., & Sobek, S. (2011). Eddy covariance flux measurements confirm extreme CH_4; emissions from a Swiss hydropower reservoir and resolve their short-term variability. *Biogeosciences*, *8*(9), 2815–2831. https://doi.org/10.5194/bg-8-2815-2011

Gash, J.H.C., & Culf, A.D. (1996). Applying a linear detrend to eddy correlation data in realtime. *Boundary Layer Meteorology*, *79*, 301-306. https://doi.org/10.1007/BF00119443

Gerling, A.B., Munger, Z.W., Doubek, J.P., Hamre, K.D., Gantzer, P.A., Little, J.C., & Carey, C.C. (2016). Whole-Catchment Manipulations of Internal and External Loading Reveal the Sensitivity of a Century-Old Reservoir to Hypoxia. *Ecosystems*, *19*(3), 555–571. https://doi.org/10.1007/s10021-015-9951-0

Golub, M., Desai, A.R., Vesala, T., Mammarella, I., Ojala, A., Bohrer, G., et. al. (2021). *New insights into diel to interannual variation in carbon dioxide emissions from lakes and reservoirs* [Preprint]. Environmental Sciences. https://doi.org/10.1002/essoar.10507313.1

Gómez-Gener, L., Rocher-Ros, G., Battin, T., Cohen, M.J., Dalmagro, H.J., Dinsmore, K.J., et. al. (2021). Global carbon dioxide efflux from rivers enhanced by high nocturnal emissions. *Nature Geoscience*, *14*(5), 289–294. https://doi.org/10.1038/s41561-021-00722-3

Gorsky, A.L., Lottig, N.R., Stoy, P.C., Desai, A.R., & Dugan, H.A. (2021). The Importance of Spring Mixing in Evaluating Carbon Dioxide and Methane Flux From a Small North-Temperate Lake in Wisconsin, United States. *Journal of Geophysical Research: Biogeosciences*, *126*(12). https://doi.org/10.1029/2021JG006537

Hanson, P.C., Pace, M.L., Carpenter, S.R., Cole, J.J., & Stanley, E.H. (2015). Integrating Landscape Carbon Cycling: Research Needs for Resolving Organic Carbon Budgets of Lakes. *Ecosystems*, *18*(3), 363–375. https://doi.org/10.1007/s10021-014-9826-9

Heiskanen, J.J., Mammarella, I., Haapanala, S., Pumpanen, J., Vesala, T., MacIntyre, S., & Ojala, A. (2014). Effects of cooling and internal wave motions on gas transfer

coefficients in a boreal lake. *Tellus B: Chemical and Physical Meteorology*, *66*(1), 22827. https://doi.org/10.3402/tellusb.v66.22827

Hounshell, A.G. (2022, December 9). aghounshell/EddyFlux: EddyFlux: Hounshell et al. 20XX re-submission-2 (Version 3.0.0). [Software] Zenodo. https://doi.org/10.5281/zenodo.742001

Howard, D.W., Hounshell, A.G., Lofton, M.E., Woelmer, W.M., Hanson, P.C., & Carey, C.C. (2021). Variability in fluorescent dissolved organic matter concentrations across diel to seasonal time scales is driven by water temperature and meteorology in a eutrophic reservoir. *Aquatic Sciences*, *83*(2), 30. https://doi.org/10.1007/s00027-021-00784-w

Huotari, J., Ojala, A., Peltomaa, E., Nordbo, A., Launiainen, S., Pumpanen, J., et. al. (2011). Long-term direct CO_2 flux measurements over a boreal lake: Five years of eddy covariance data. *Geophysical Research Letters*, *38*(18). https://doi.org/10.1029/2011GL048753

Hyndman, R.J. & Athanasopoulos, G. (2018). *Forecasting: principles and practice*, 2nd Edition. Otexts, Melbourne, Australia.

Hyndman, R., Athanasopoulos, G., Bergmeir, C., Caceres, G., Chhay, L., O'Hara-Wild, M., et al. (2022, January 10). forecast: Forecasting functions for time series and linear models. (Version 8.16). [Software]. R Package. https://pkg.robjhyndman.com/forecast/

Hyndman, R. J., & Khandakar, Y. (2008). Automatic Time Series Forecasting: The **forecast** Package for *R*. *Journal of Statistical Software*, *27*(3). https://doi.org/10.18637/jss.v027.i03

Imrit, M.A., & Sharma, S. (2021). Climate Change is Contributing to Faster Rates of Lake Ice Loss in Lakes Around the Northern Hemisphere. *Journal of Geophysical Research: Biogeosciences*, *126*(7). https://doi.org/10.1029/2020JG006134

Jammet, M., Crill, P., Dengel, S., & Friborg, T. (2015). Large methane emissions from a subarctic lake during spring thaw: Mechanisms and landscape significance: Lake

methane emissions among spring thaw. *Journal of Geophysical Research: Biogeosciences*, *120*(11), 2289–2305. https://doi.org/10.1002/2015JG003137

Jammet, M., Dengel, S., Kettner, E., Parmentier, F.J.W., Wik, M., Crill, P., & Friborg, T. (2017). Year-round CH_4 and CO_2 flux dynamics in two contrasting freshwater ecosystems of the subarctic. *Biogeosciences*, *14*(22), 5189–5216. https://doi.org/10.5194/bg-14-5189-2017

Jonsson, A., Åberg, J., Lindroth, A., & Jansson, M. (2008). Gas transfer rate and CO_2 flux between an unproductive lake and the atmosphere in northern Sweden: CO_2 emission in an unproductive lake. *Journal of Geophysical Research: Biogeosciences*, *113*(G4). https://doi.org/10.1029/2008JG000688

Klaus, M., Seekell, D.A., Lidberg, W., & Karlsson, J. (2019). Evaluations of Climate and Land Management Effects on Lake Carbon Cycling Need to Account for Temporal Variability in CO_2 Concentrations. *Global Biogeochemical Cycles*, *33*(3), 243–265. https://doi.org/10.1029/2018GB005979

Kljun, N., Calanca, P., Rotach, M.W., & Schmid, H.P. (2015). A simple two-dimensional parameterisation for Flux Footprint Prediction (FFP). *Geoscientific Model Development*, *8*(11), 3695–3713. https://doi.org/10.5194/gmd-8-3695-2015

Kljun, N., Rotach, M.W., & Schmid, H.P. (2002). A Three-Dimensional Backward Lagrangian Footprint Model For A Wide Range Of Boundary-Layer Stratifications. *Boundary-Layer Meteorology*, *103*(2), 205–226. https://doi.org/10.1023/A:1014556300021

Lee, X., Massman, W., & Law B. (Eds.). (2005). *Handbook of Micrometeorology A Guide for Surface Flux Measurement and Analysis*, United States of America:Springer Science + Business Media, Inc.

LiCor Biogeosciences. (2019, December 18). EddyPro® Software (Version 7.0.6) [Software]. LI-COR. https://www.licor.com/env/support/EddyPro/home.html

Liu, H., Zhang, Q., Katul, G.G., Cole, J.J., Chapin, F.S., & MacIntyre, S. (2016). Large CO_2 effluxes at night and during synoptic weather events significantly contribute to CO_2

emissions from a reservoir. *Environmental Research Letters*, *11*(6), 064001. https://doi.org/10.1088/1748-9326/11/6/064001

Lofton, M.E. (2022). melofton/FCR-phytos: Lofton et al. 20XX manuscript second revision (Version 3.0.0.). [Software]. Zenodo. https://doi.org/10.5281/zenodo.6483433

Loken, L. C., Crawford, J.T., Schramm, P.J., Stadler, P., Desai, A.R., & Stanley, E.H. (2019). Large Spatial and Temporal Variability of Carbon Dioxide and Methane in a Eutrophic Lake. *Journal of Geophysical Research: Biogeosciences*, *124*(7), 2248–2266. https://doi.org/10.1029/2019JG005186

MacIntyre, S., Jonsson, A., Jansson, M., Aberg, J., Turney, D.E., & Miller, S.D. (2010). Buoyancy flux, turbulence, and the gas transfer coefficient in a stratified lake. *Geophysical Research Letters*, *37*(24). https://doi.org/10.1029/2010GL044164

Mammarella, I., Nordbo, A., Rannik, Ü., Haapanala, S., Levula, J., Laakso, H., et. al. (2015). Carbon dioxide and energy fluxes over a small boreal lake in Southern Finland. *Journal of Geophysical Research: Biogeosciences*, *120*(7), 1296–1314. https://doi.org/10.1002/2014JG002873

Mauder, M., & Foken T. (2006). Impact of post-field data processing on eddy covariance flux estimates and energy balance closure. *Meteorologische Zietschrift, 15*, 597-609.

McClure, R.P., Hamre, K.D., Niederlehner, B.R., Munger, Z.W., Chen, S., Lofton, M.E., Schreiber, M.E., & Carey, C.C. (2018). Metalimnetic oxygen minima alter the vertical profiles of carbon dioxide and methane in a managed freshwater reservoir. *Science of The Total Environment*, *636*, 610–620. https://doi.org/10.1016/j.scitotenv.2018.04.255

McClure, R.P., Lofton, M.E., Chen S., Krueger, K.M., Little, J.C., & Carey, C.C. (2020). The Magnitude and Drivers of Methane Ebullition and Diffusion Vary on a Longitudinal Gradient in a Small Freshwater Reservoir. *Journal of Geophysical Research: Biogeosciences*, 125. https://doi.org/10.1029/2019JG005205

McClure, R.P., Schreiber, M.E., Lofton, M.E., Chen, S., Krueger, K.M., & Carey, C.C. (2021). Ecosystem-Scale Oxygen Manipulations Alter Terminal Electron Acceptor Pathways in a

Eutrophic Reservoir. *Ecosystems*, *24*(6), 1281–1298. https://doi.org/10.1007/s10021-020-00582-9

McDermitt, D., Burba, G., Xu, L., Anderson, T., Komissarov, A., Riensche, B., et al. (2011). A new low-power, open-path instrument for measuring methane flux by eddy covariance. *Applied Physics B*, 102: 391-405. https://doi.org/10.1007/s00340-010-4307-0

Moncrieff, J.B., Clement, R., Finnigan, J., Meyers, T. (2004). Averaging, Detrending, and Filtering of Eddy Covariance Time Series. In: Lee X., Massman W., Law B. (eds) *Handbook of Micrometeorology*. (Vol 29, pp. 7-31). Springer, Dordrecht. https://doi.org/10.1007/1-4020-2265-4_2

Moncrieff, J.B., Massheder, J.M.,de Bruin, H., Ebers, J., Friborg, T., Heusinkveld, B., et al. (1997). A system to measure surface fluxes of momentum, sensible heat, water vapor, and carbon dioxide. *Journal of Hydrology,* 188-189: 598-611. https://doi.org/10.1016/S0022-1694(96)03194-0

Ouyang, Z., Shao, C., Chu, H., Becker, R., Bridgeman, T., Stepien, C., John, R., & Chen, J. (2017). The Effect of Algal Blooms on Carbon Emissions in Western Lake Erie: An Integration of Remote Sensing and Eddy Covariance Measurements. *Remote Sensing*, *9*(1), 44. https://doi.org/10.3390/rs9010044

Podgrajsek, E., Sahlée, E., Bastviken, D., Holst, J., Lindroth, A., Tranvik, L., & Rutgersson, A. (2014). Comparison of floating chamber and eddy covariance measurements of lake greenhouse gas fluxes. *Biogeosciences*, *11*(15), 4225–4233. https://doi.org/10.5194/bg-11-4225-2014

Podgrajsek, E., Sahlée, E., Bastviken, D., Natchimuthu, S., Kljun, N., Chmiel, H.E., Klemedtsson, L., & Rutgersson, A. (2016). Methane fluxes from a small boreal lake measured with the eddy covariance method. *Limnology and Oceanography*, *61*(S1), S41–S50. https://doi.org/10.1002/lno.10245

Prairie, Y.T., Alm, J., Beaulieu, J., Barros, N., Battin, T., Cole, J., et. al. (2018). Greenhouse Gas Emissions from Freshwater Reservoirs: What Does the Atmosphere See? *Ecosystems*, *21*(5), 1058–1071. https://doi.org/10.1007/s10021-017-0198-9

Read, J.S., Hamilton, D.P., Desai, A.R., Rose, K.C., MacIntyre, S., Lenters, J.D., et al. (2012). Lake-size dependency of wind shear and convection as controls on gas exchange: lake-size dependency of u_* and w_*. *Geophysical Research Letters*, *39*(9). https://doi.org/10.1029/2012GL051886

Reed, D.E., Dugan, H.A., Flannery, A.L., & Desai, A.R. (2018). Carbon sink and source dynamics of a eutrophic deep lake using multiple flux observations over multiple years. *Limnology and Oceanography Letters*, *3*(3), 285–292. https://doi.org/10.1002/lol2.10075

Rosentreter, J.A., Borges, A.V., Deemer, B.R., Holgerson, M.A., Liu, S., Song, C., et al. (2021). Half of global methane emissions come from highly variable aquatic ecosystem sources. *Nature Geoscience*, *14*(4), 225–230. https://doi.org/10.1038/s41561-021-00715-2

Sanches, L.F., Guenet, B., Marinho, C.C., Barros, N., & de Assis Esteves, F. (2019). Global regulation of methane emission from natural lakes. *Scientific Reports*, *9*(1), 255. https://doi.org/10.1038/s41598-018-36519-5

Scholz, K., Ejarque, E., Hammerle, A., Kainz, M., Schelker, J., & Wohlfahrt, G. (2021). Atmospheric CO_2 Exchange of a Small Mountain Lake: Limitations of Eddy Covariance and Boundary Layer Modeling Methods in Complex Terrain. *Journal of Geophysical Research: Biogeosciences*, *126*(7). https://doi.org/10.1029/2021JG006286

Schubert, C.J., Diem, T., & Eugster, W. (2012). Methane Emissions from a Small Wind Shielded Lake Determined by Eddy Covariance, Flux Chambers, Anchored Funnels, and Boundary Model Calculations: A Comparison. *Environmental Science & Technology*, *46*(8): 4515-4522. https://doi.org/10.1021/es203465x

Shao, C., Chen, J., Stepien, C.A., Chu, H., Ouyang, Z., Bridgeman, T.B., Czajkowski, K.P., Becker, R.H., & John, R. (2015). Diurnal to annual changes in latent, sensible heat, and CO_2 fluxes over a Laurentian Great Lake: A case study in Western Lake Erie. *Journal of*

Geophysical Research: Biogeosciences, *120*(8), 1587–1604. https://doi.org/10.1002/2015JG003025

Sharma, S., Richardson, D.C., Woolway, R.I., Imrit, M.A., Bouffard, D., Blagrave, K., et. al. (2021). Loss of Ice Cover, Shifting Phenology, and More Extreme Events in Northern Hemisphere Lakes. *Journal of Geophysical Research: Biogeosciences*, *126*(10). https://doi.org/10.1029/2021JG006348

Sieczko, A. K., Duc, N.T., Schenk, J., Pajala, G., Rudberg, D., Sawakuchi, H.O., & Bastviken, D. (2020). Diel variability of methane emissions from lakes. *Proceedings of the National Academy of Sciences*, *117*(35), 21488–21494. https://doi.org/10.1073/pnas.2006024117

Smith, S.V., Renwick, W.H., Bartley, J.D., & Buddemeier, R.W. (2002). Distribution and significance of small, artificial water bodies across the United States landscape. *Science of The Total Environment*, *299*(1–3), 21–36. https://doi.org/10.1016/S0048-9697(02)00222-X

Sobek, S., Tranvik, L.J., & Cole, J.J. (2005). Temperature independence of carbon dioxide supersaturation in global lakes: Carbon dioxide supersaturation in global lakes. *Global Biogeochemical Cycles*, *19*(2),. https://doi.org/10.1029/2004GB002264

Soloviev, A., Donelan, M., Graber, H., Haus, B., & Schlüssel, P. (2007). An approach to estimation of near-surface turbulence and CO_2 transfer velocity from remote sensing data. *Journal of Marine Systems*, *66*(1–4), 182–194. https://doi.org/10.1016/j.jmarsys.2006.03.023

Taoka, T., Iwata, H., Hirata, R., Takahashi, Y., Miyabara, Y., & Itoh, M. (2020). Environmental Controls of Diffusive and Ebullitive Methane Emissions at a Subdaily Time Scale in the Littoral Zone of a Midlatitude Shallow Lake. *Journal of Geophysical Research: Biogeosciences*, *125*(9). https://doi.org/10.1029/2020JG005753

Tranvik, L.J., Downing, J.A., Cotner, J.B., Loiselle, S.A., Striegl, R.G., Ballatore, T.J., et. al. (2009). Lakes and reservoirs as regulators of carbon cycling and climate. *Limnology and Oceanography*, *54*(6part2), 2298–2314. https://doi.org/10.4319/lo.2009.54.6_part_2.2298

USACE (United States Army Corps of Engineers). (2021). National inventory of Dams (NID). [accessed 2022 February 7]. https://nid.usace.army.mil/#/

Vachon, D., & Prairie, Y.T. (2013). The ecosystem size and shape dependence of gas transfer velocity versus wind speed relationships in lakes. *Canadian Journal of Fisheries and Aquatic Sciences*, *70*(12), 1757–1764. https://doi.org/10.1139/cjfas-2013-0241

Vesala, T., Eugster, W., & Ojala, A. (2012). Eddy Covariance Measurements over Lakes. In M. Aubinet, T. Vesala, & D. Papale (Eds.), *Eddy Covariance* (pp. 365–376). Springer Netherlands. https://doi.org/10.1007/978-94-007-2351-1_15

Vesala, T., Huotari, J., Rannik, Ü., Suni, T., Smolander, S., Sogachev, A., Launiainen, S., & Ojala, A. (2006). Eddy covariance measurements of carbon exchange and latent and sensible heat fluxes over a boreal lake for a full open-water period. *Journal of Geophysical Research*, *111*(D11), D11101. https://doi.org/10.1029/2005JD006365

Vickers, D., & Mahrt, L. (1997). Quality Control and Flux Sampling Problems for Tower and Aircraft Data. *Journal of Atmospheric and Oceanic Technology*, *14*(3), 512–526. https://doi.org/10.1175/1520-0426(1997)014<0512:QCAFSP>2.0.CO;2

Waldo, S., Beaulieu, J.J., Barnett, W., Balz, D. A., Vanni, M.J., Williamson, T., & Walker, J.T. (2021). Temporal trends in methane emissions from a small eutrophic reservoir: The key role of a spring burst. *Biogeosciences*, *18*(19), 5291–5311. https://doi.org/10.5194/bg-18-5291-2021

Wanninkhof, R., Asher, W.E., Ho, D.T., Sweeney, C., & McGillis, W.R. (2009). Advances in Quantifying Air-Sea Gas Exchange and Environmental Forcing. *Annual Review of Marine Science*, 1: 213-244. https://doi.org/10.1146/annurev.marine.010908.163742

Watras, C.J., Morrison, K.A., Crawford, J.T., McDonald, C.P., Oliver, S.K., & Hanson, P.C. (2015). Diel cycles in the fluorescence of dissolved organic matter in dystrophic Wisconsin seepage lakes: Implications for carbon turnover: Diel CDOM fluorescence cycles. *Limnology and Oceanography*, *60*(2), 482–496. https://doi.org/10.1002/lno.10026

Webb, E.K., Pearman, G.I., & Leuning R. (1980). Correction of flux measurements for density effects due to heat and water vapour transfer. *Quarterly Journal of the Royal Meteorological Society*, *106*(447), 85-100. https://doi.org/10.1002/qj.49710644707

Wik, M., Thornton, B.F., Bastviken, D., Uhlbäck, J., & Crill, P.M. (2016). Biased sampling of methane release from northern lakes: A problem for extrapolation. *Geophysical Research Letters*, *43*(3), 1256–1262. https://doi.org/10.1002/2015GL066501

Wilczak, J.M., Oncley, S.P., Stage, S.A. (2001). Sonic anemometer tilt correction algorithms. *Boundary-Layer Meteorology*, 99, 127-150. https://doi.org/10.1023/A:1018966204465

Winslow, L. A., Read, J.S., Hanson, P.C., & Stanley, E.H. (2014). Lake shoreline in the contiguous United States: Quantity, distribution and sensitivity to observation resolution. *Freshwater Biology*, *59*(2), 213–223. https://doi.org/10.1111/fwb.12258

Winslow, L., Read, J., Woolway, R., Brentrup, J., Leach T., Zwart, J., Albers, S., & Collinge, C. (2016a, June 9). LakeAnalyzer: Lake Physics Tools. (Version 1.11.4.1). [Software]. R. Package. https://CRAN.R-project.org/package=rLakeAnalyzer

Winslow, L.A., Zwart, J.A., Batt, R.D., Dugan, H.A., Woolway, R.I., Corman, J.R., Hanson, P.C., & Read, J.S. (2016c). LakeMetabolizer: An R package for estimating lake metabolism from free-water oxygen using diverse statistical models. *Inland Waters*, *6*(4), 622–636. https://doi.org/10.1080/IW-6.4.883

Winslow, L., Zwart, J., Batt, R., Corman, J., Dugan, H., Hanson, P., et. al. (2016b, June 23). LakeMetabolizer: Tools for the analysis of ecosystem metabolism. (Version 1.5.0). [Software]. R Package. https://CRAN.R-project.org/pacakge=LakeMetabolizer

Woolway, R.I., Kraemer, B.M., Lenters, J.D., Merchant, C.J., O'Reilly, C.M., & Sharma, S. (2020). Global lake responses to climate change. *Nature Reviews Earth & Environment*, *1*(8), 388–403. https://doi.org/10.1038/s43017-020-0067-5

Wutzler, T., Lucas-Moffat, A., Migliavacca, M., Knauer, J., Sickel, K., Šigut, L., Menzer, O., & Reichstein, M. (2018). Basic and extensible post-processing of eddy covariance flux data

with REddyProc. *Biogeosciences*, *15*(16), 5015–5030. https://doi.org/10.5194/bg-15-5015-2018

Wutzler, T., Reichstein, M., Lucas-Moffat, A.M., Menzer, O., Migliavacca, M., & Sickel, K. (2021, December 01). REddyProc: Post Processing of (Half-) Hourly Eddy-Covariance Measurements. (Version 1.3.1). [Software]. R. Package. https://CRAN.R-project.org/package=REddyProc

Supporting Information for

Eddy covariance data reveal that a small freshwater reservoir emits a substantial amount of carbon dioxide and methane

Alexandria G. Hounshell[1, †], Brenda M. D'Acunha[2], Adrienne Breef-Pilz[1], Mark S. Johnson[2,3], R. Quinn Thomas[1,4], Cayelan C. Carey[1]

[1] Department of Biological Sciences, Virginia Tech, Blacksburg, VA, USA, [2] Department of Earth, Ocean, and Atmospheric Sciences, University of British Columbia, Vancouver, BC, Canada, [3] Institute for Resources, Environment and Sustainability, University of British Columbia, Vancouver, BC, Canada, [4] Department of Forest Resources and Environmental Conservation, Virginia Tech, Blacksburg, VA, USA

Corresponding author: Alexandria G. Hounshell (alexgh@vt.edu)

† Current affiliation: National Centers for Coastal Ocean Science, National Oceanographic and Atmospheric Administration, Beaufort, NC, 28516, alexandria.hounshell@noaa.gov

Contents of this file

Introduction

The supplementary information additional figures (Figures S1-S13) and tables (Tables S1-S11) used as supporting information in the associated manuscript.

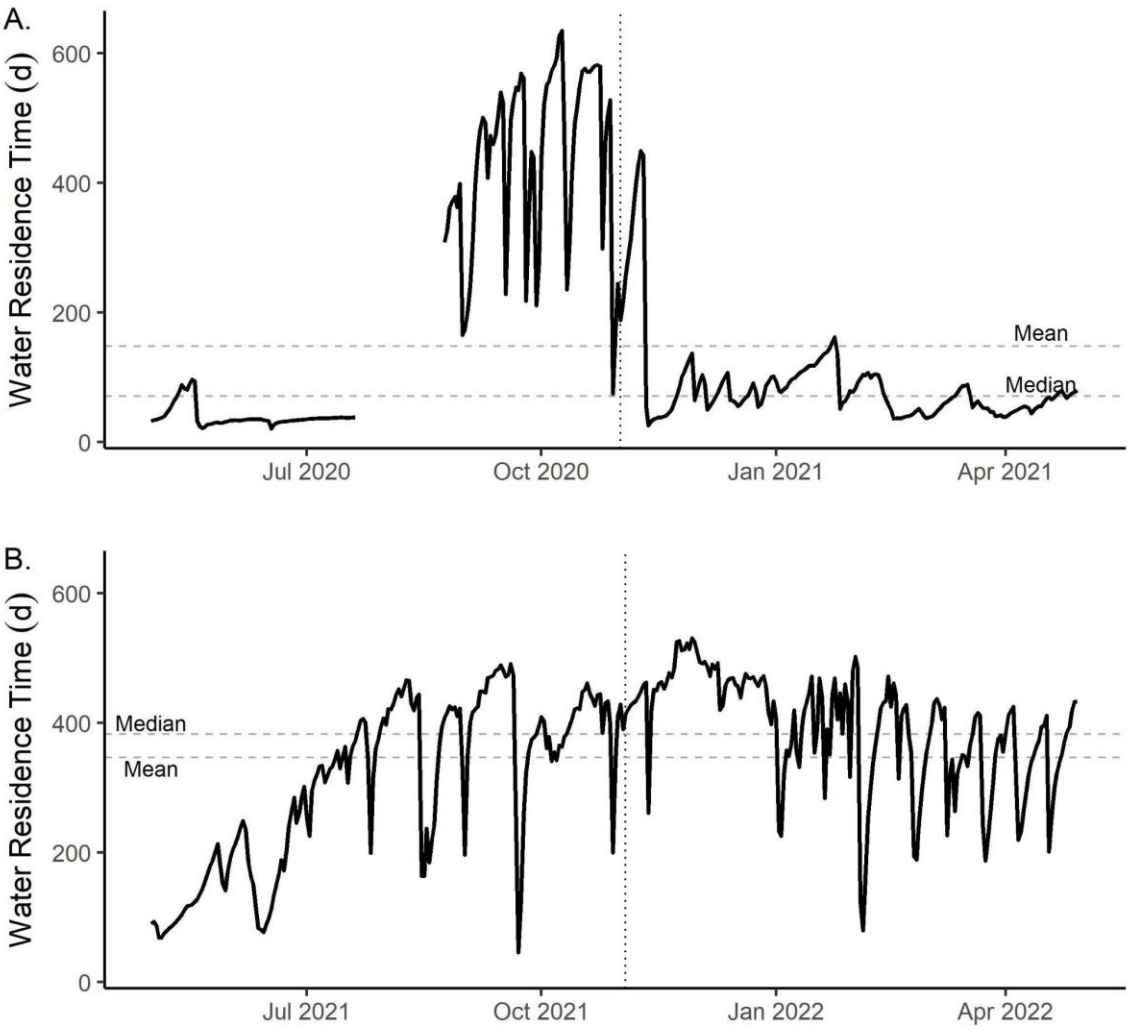

Fig. S1. Water residence time (days, d) plotted for A. Year 1 (May 2020-April 2021) and B. Year 2 (May 2021-April 2022). The vertical dashed line represents fall turnover for each year. The horizontal dashed lines correspond to the mean and median, respectively (Year 1: mean = 148 d, median = 71 d; Year 2: mean = 347 d, median = 383 d).

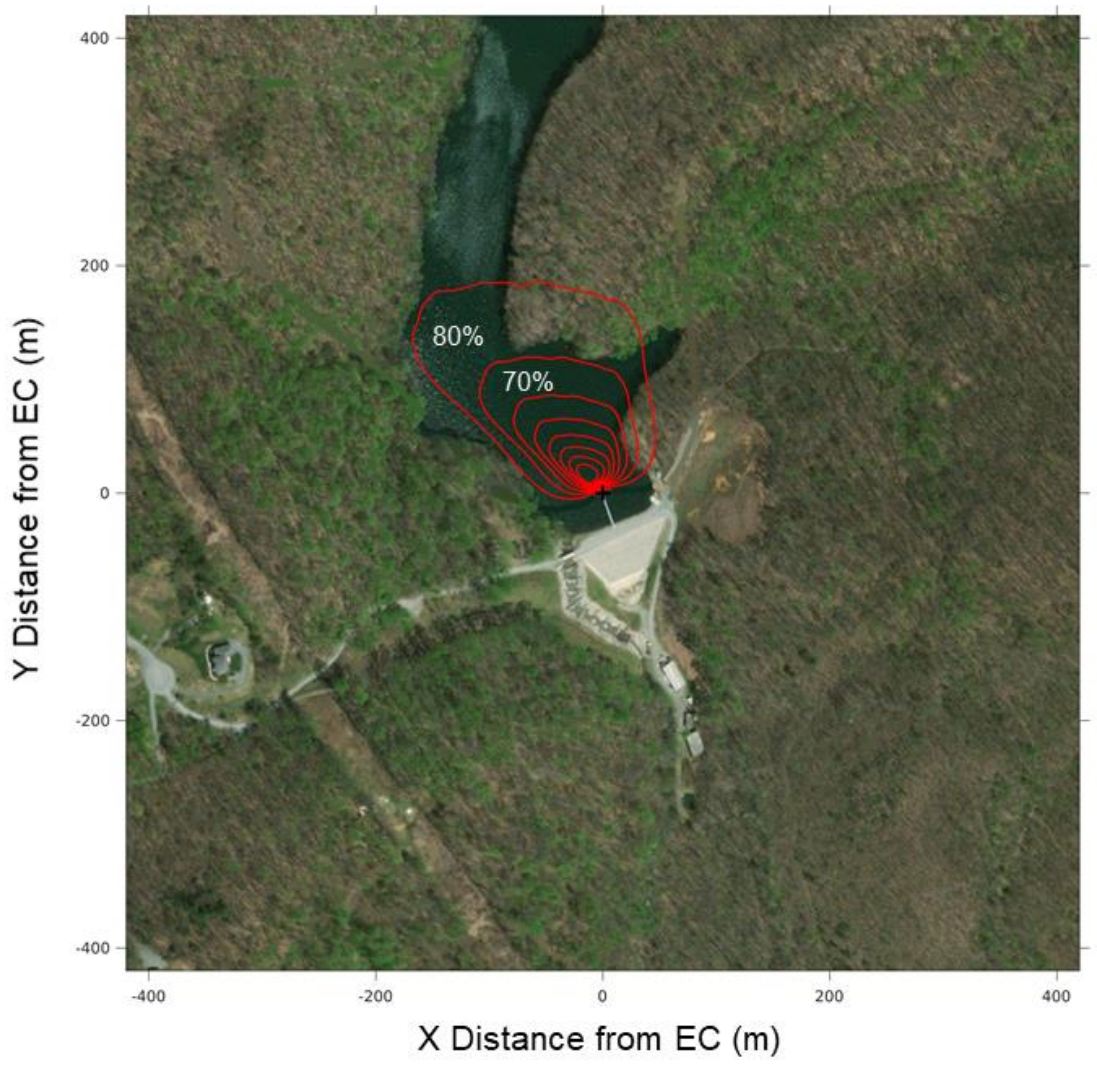

Figure S2. Cumulative footprint for fluxes retained for analysis during the two years of eddy covariance (EC) fluxes measured from Falling Creek Reservoir following methods in Kljun et al. (2015). The 10-80% isolines are plotted as red circles around the EC system (denoted as the black plus-sign). Additional data filtering was conducted to remove fluxes within the 80% isoline which originated over land.

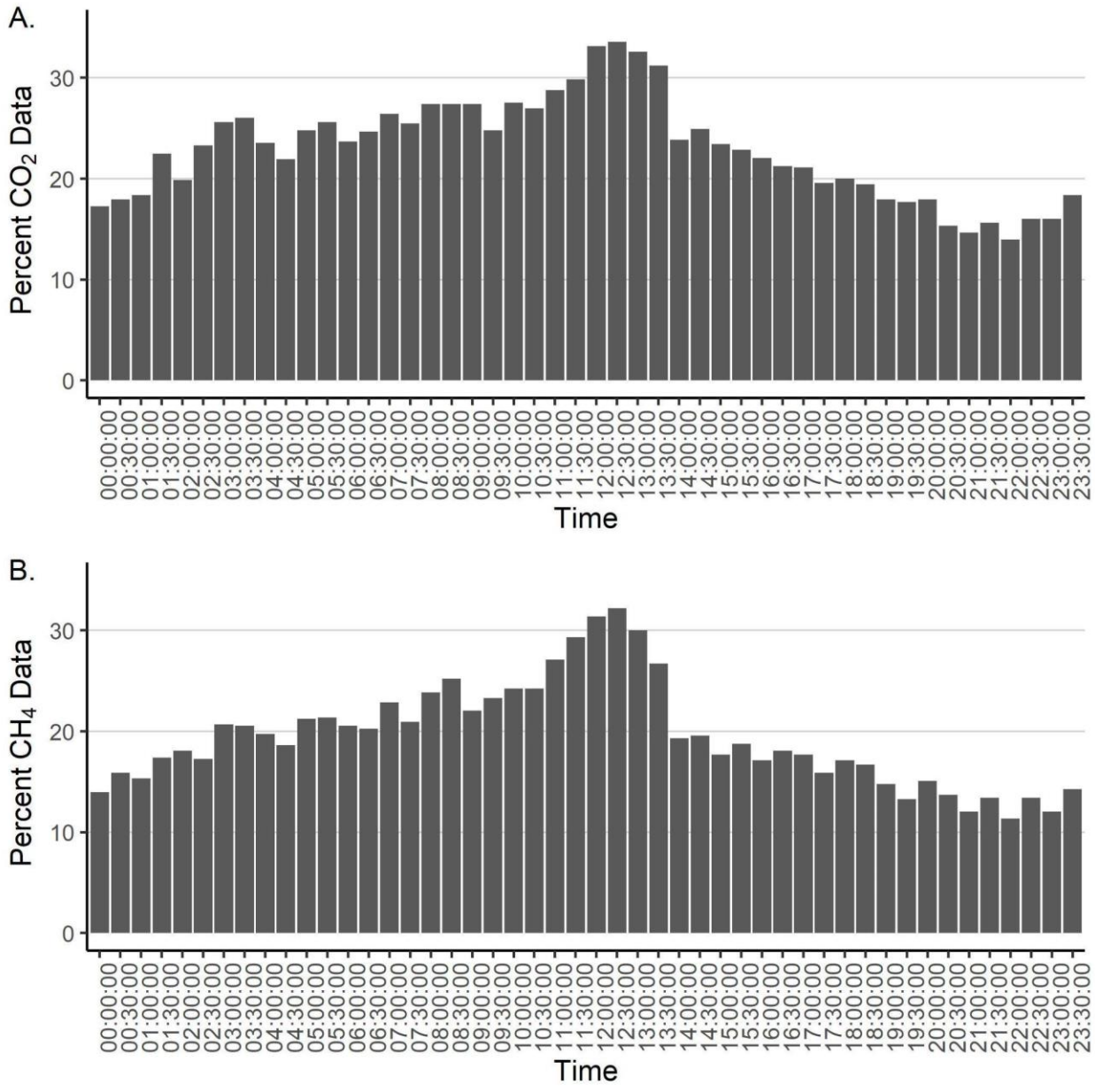

Figure S3. Barplot of average percent of data availability for A. carbon dioxide (CO_2) and B. methane (CH_4) fluxes distributed throughout the day (half-hourly from 0:00 to 23:30).

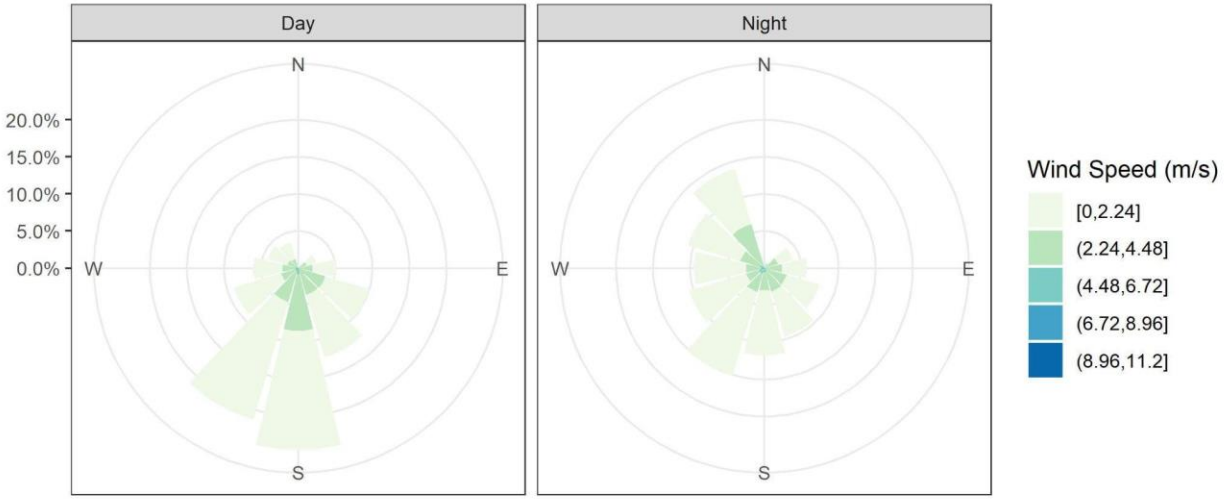

Figure S4. Windrose of all measured windspeed and direction during the study period separated by A. Day (shortwave radiation in > 0 W m^2) and B. Night (shortwave radiation in < 0 W m^2) collected from the meteorological stations deployed at the dam.

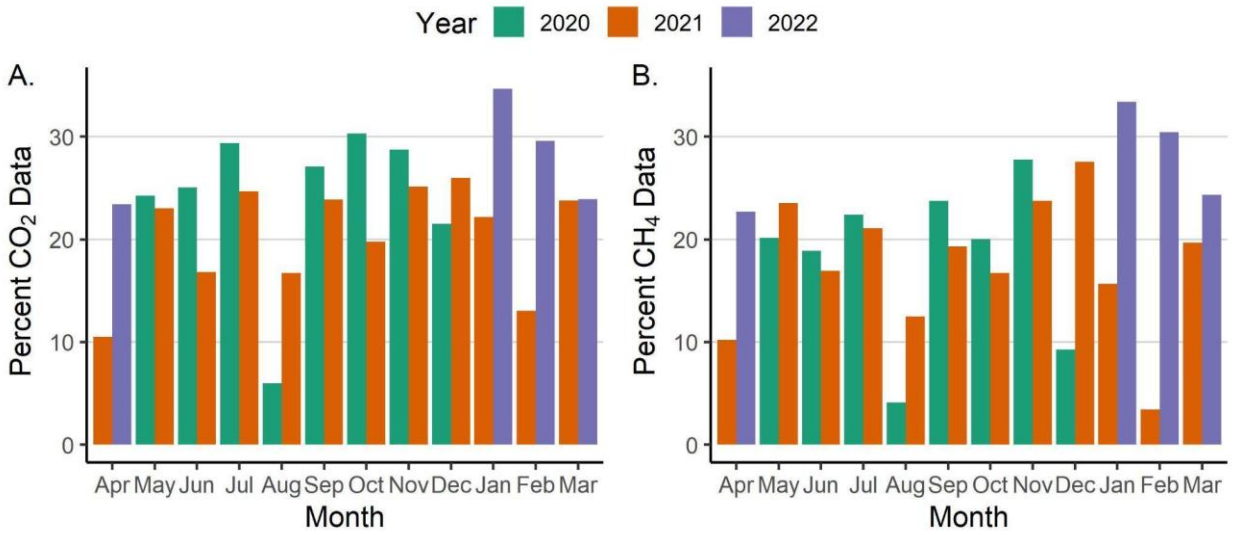

Figure S5. Barplot of average percent of data availability for A. carbon dioxide (CO_2) and B. methane (CH_4) fluxes distributed throughout each month and year of the study period.

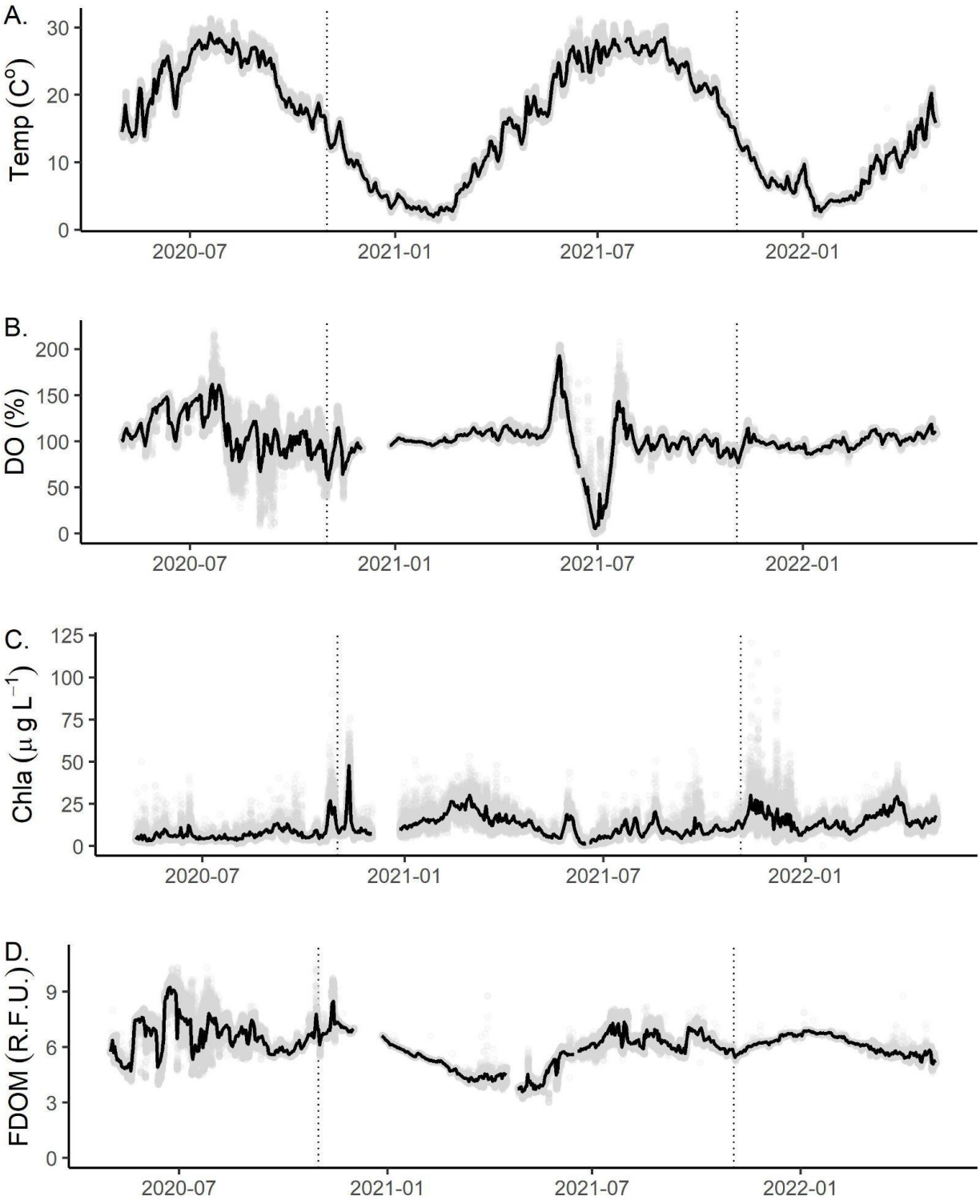

Figure S6. Environmental variables measured during the study period, including A. Surface Water Temperature (Temp, °C) measured at 0.1 m below the surface; B. Dissolved oxygen (DO, percent saturation, %) measured at 1.6 m; C. Chlorophyll-*a* (Chl-a, µg L^{-1})

measured at 1.6 m; and D. fluorescent dissolved organic matter (fDOM, Relative Fluorescence Units, RFU) measured at 1.6 m. Solid black lines represent the daily mean while the light grey points represent individual measurements made every 15 minutes for inflow and every 10 minutes for all other variables. The dashed vertical black line indicates reservoir fall turnover for both years.

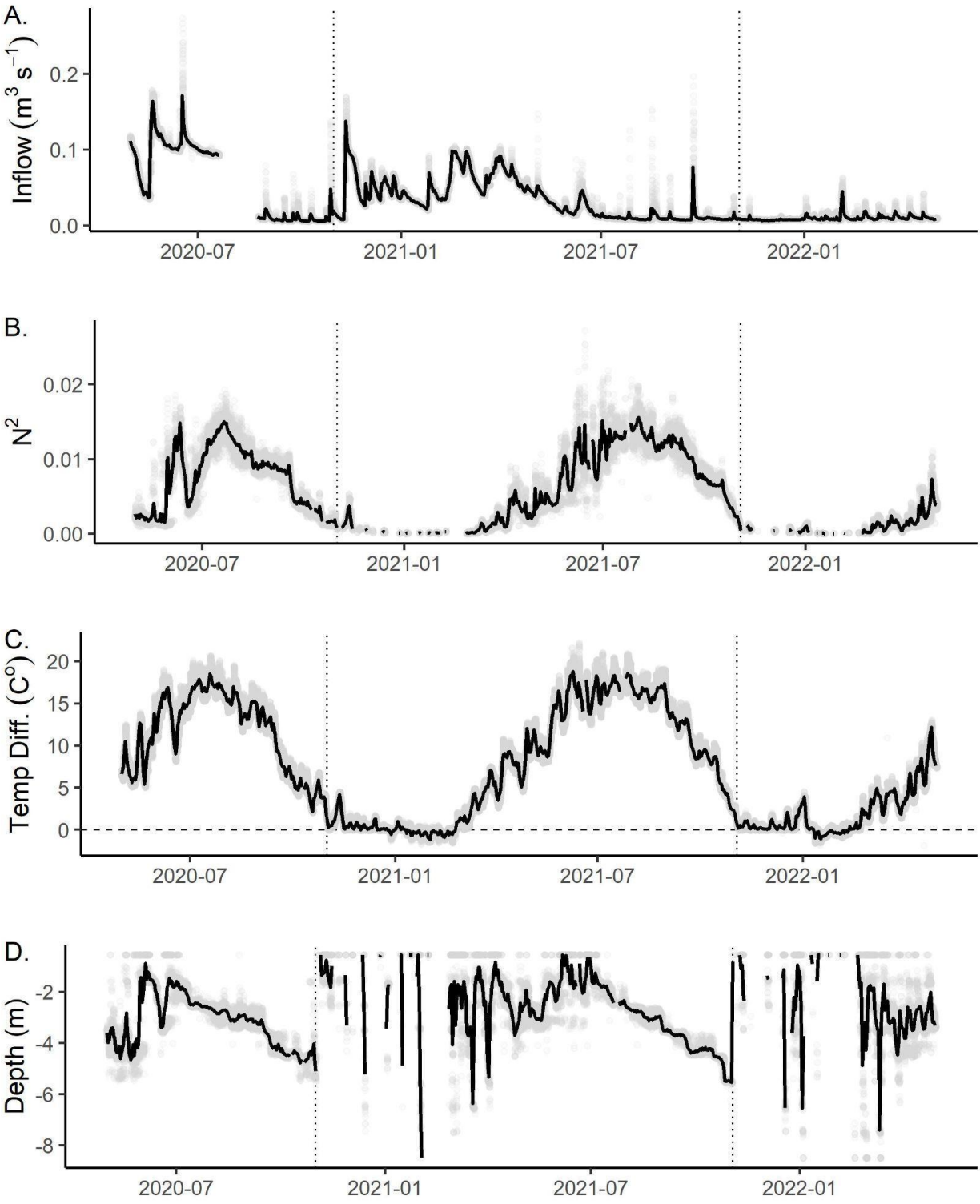

Figure S7. Environmental variables measured during the study period, including A. Inflow (m^3 s^{-1}) measured at the primary inflow to Falling Creek Reservoir; B. Buoyancy frequency (N^2) calculated from thermal profiles at the deepest point in the reservoir; C.

The temperature difference (Temp Diff., °C) measured from the surface (0.1 m) and bottom (9 m) at the deepest point of the reservoir; and D. Thermocline depth (Depth, m) calculated from thermal profiles deployed at the deepest point of the reservoir. Solid black lines represent the daily mean while the light grey points represent individual measurements made every 15 minutes for inflow and every 10 minutes for all other variables. The dashed vertical black line indicates reservoir fall turnover for each year.

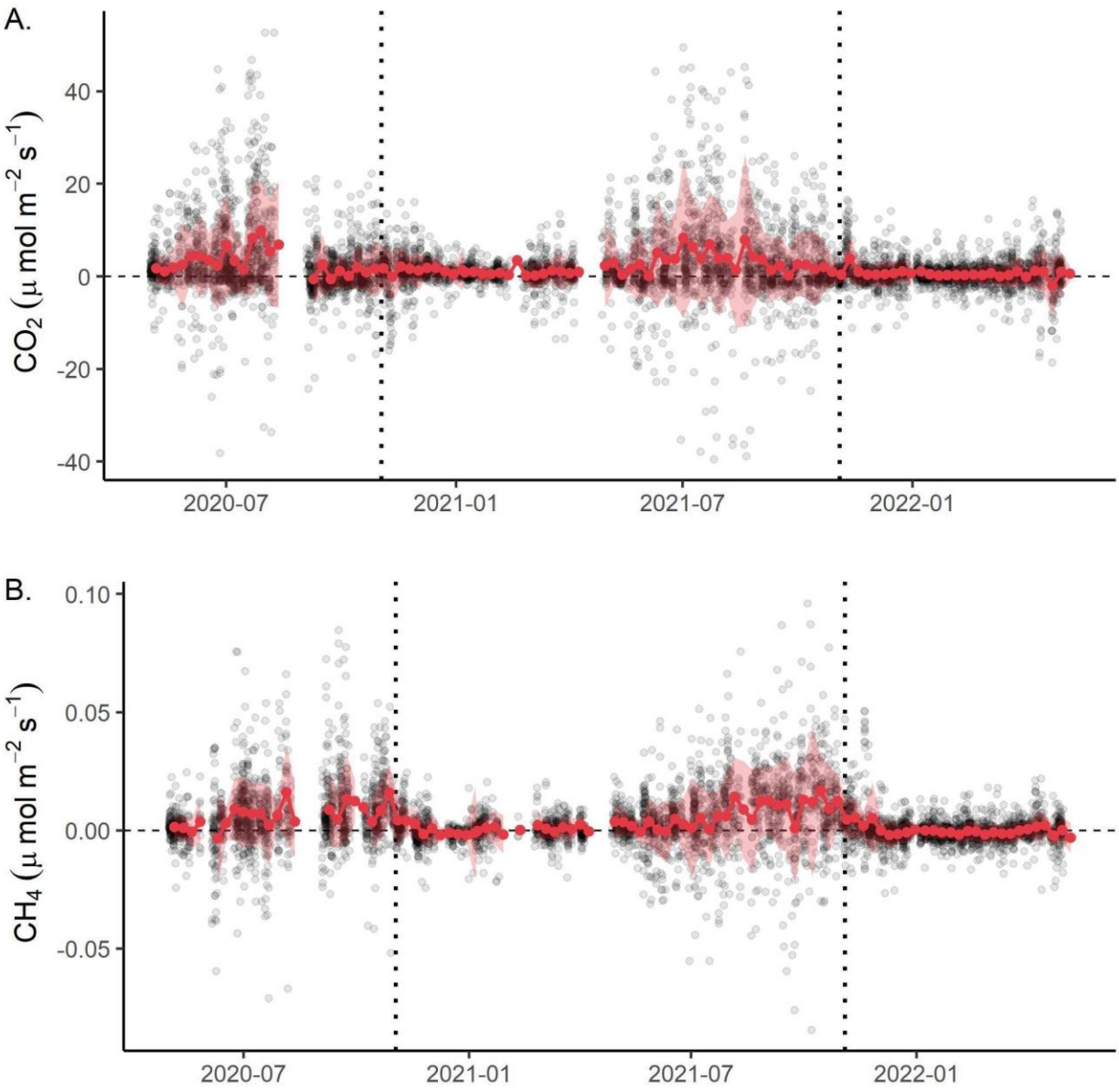

Figure S8. A. Mean weekly carbon dioxide fluxes (CO_2, μmol m^{-2} s^{-1}) and B. mean weekly methane fluxes (CH_4, μmol m^{-2} s^{-1}) aggregated from measured eddy covariance data from 1 May 2020 to 30 April 2021 in Falling Creek Reservoir plotted as a red line with dots. The red shaded area corresponds to the standard deviation (±1 S.D.) of aggregated fluxes for both measured and gap-filled values. Black dots represent measured half-hourly fluxes. The vertical dashed line corresponds to reservoir fall turnover for each year.

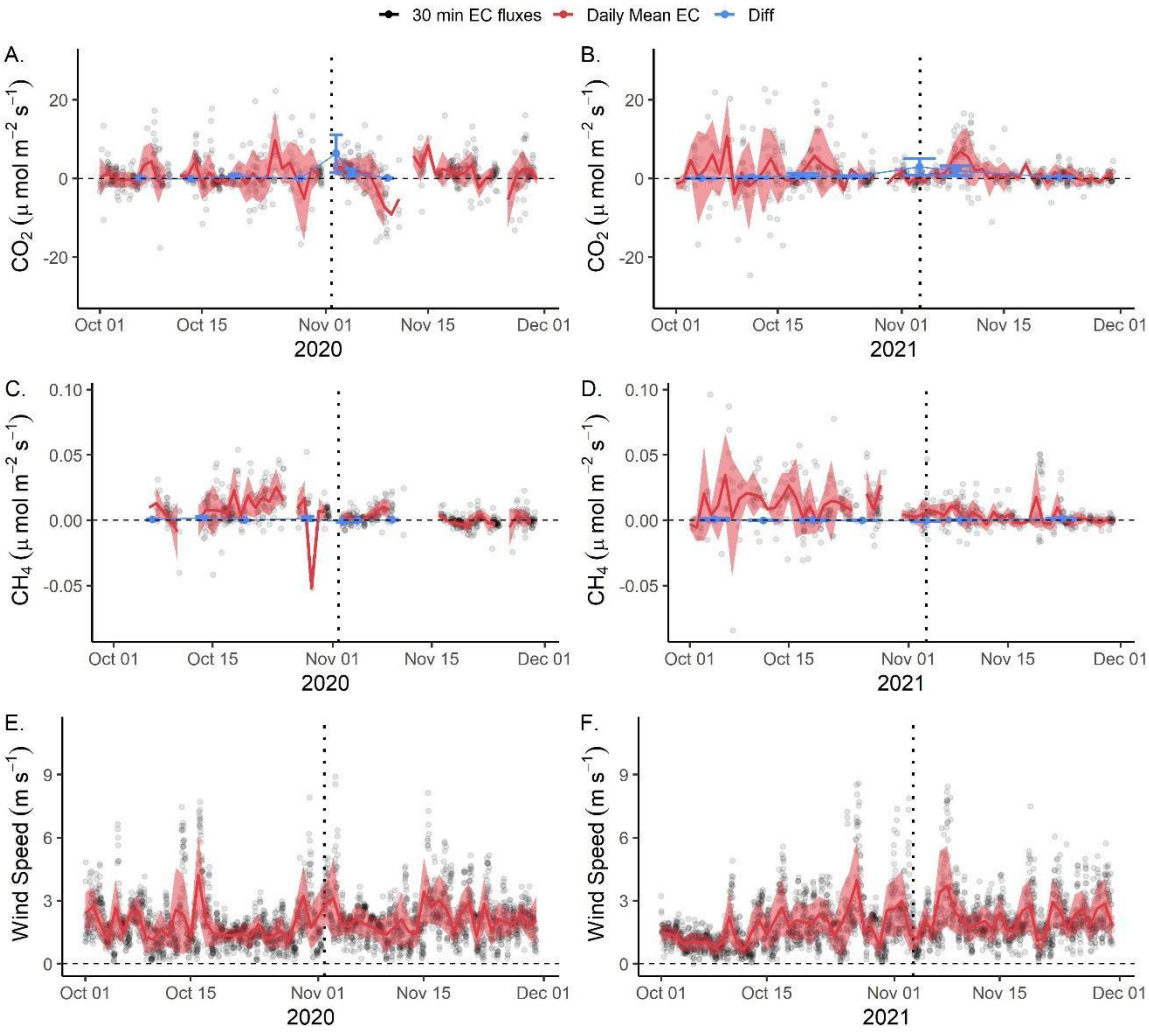

Figure S9. Mean daily A., B. Carbon dioxide (CO_2, μmol m^{-2} s^{-1}) and C., D. Mean daily methane fluxes (CH_4 μmol m^{-2} s^{-1}) for 2020 and 2021, respectively, around reservoir fall turnover (01 November 2021 and 03 November 2022, respectively). Mean daily wind is also plotted for E. 2020 and F. 2021. Grey dots represent measured half-hourly fluxes from the EC system (CO_2, CH_4) and the meteorological station deployed at the dam of Falling Creek Reservoir (Wind speed). The dark red line represents daily mean fluxes or wind speed. The shaded red area represents ±1 standard deviation of the daily 30-minute fluxes or wind speed. The vertical dotted line indicates reservoir fall turnover.

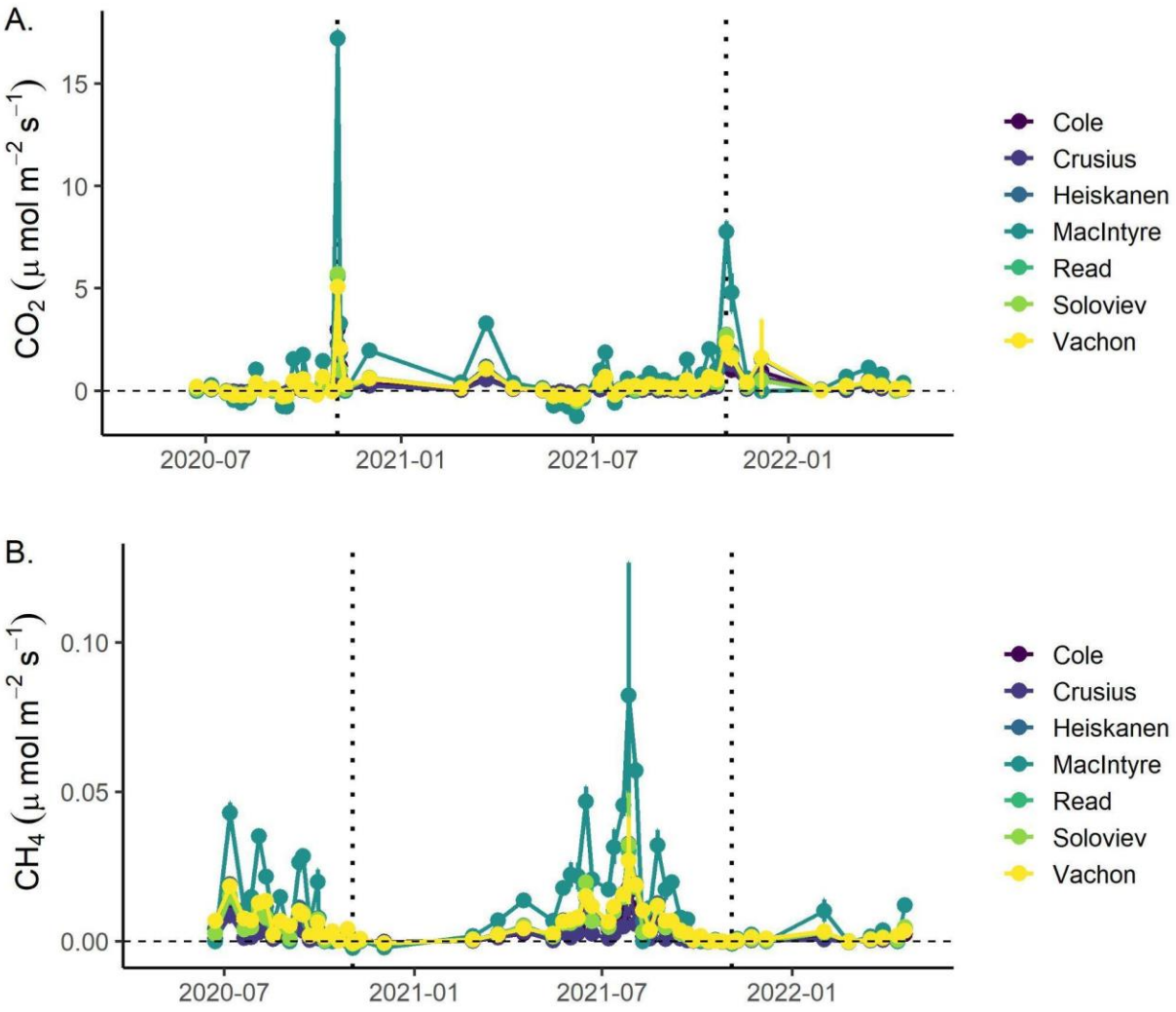

Figure S10. Discrete diffusive fluxes calculated for A. carbon dioxide (CO_2, µmol m^{-2} s^{-1}) and B. methane (CH_4, µmol m^{-2} s^{-1}) during the study period (1 May 2020 to 30 April 2022) using multiple gas transfer coefficient models (k; Winslow et al. 2016; Cole and Caraco, 1998; Crusius and Wannikof, 2003; Vachon and Prairie, 2013; MacIntyre et al. 2010; Heiskanen et al. 2014; Read et al. 2012; Soloviev et al. 2007). Points represent the mean of two replicates calculated for each k method and the error bars are the standard deviation (±1 S.D.). The dashed horizontal line indicates zero fluxes and the dotted vertical line corresponds to reservoir fall turnover on 1 November 2020 and 3 November 2021, respectively.

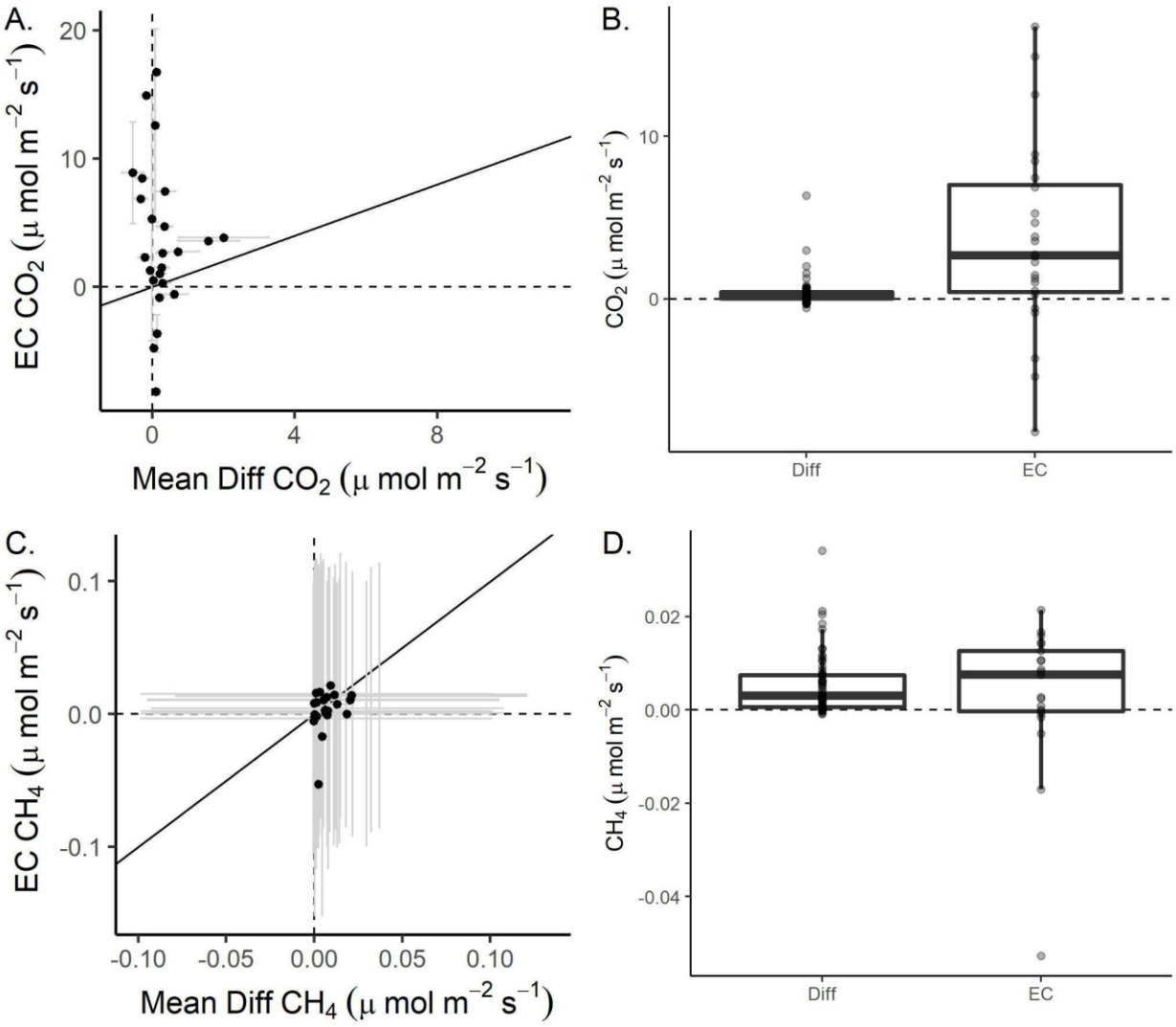

Figure S11. Instantaneous mean diffusive fluxes compared to mean hourly fluxes obtained using the eddy covariance (EC) system for A. carbon dioxide (CO_2, μmol m^{-2} s^{-1}; n = 24 observations) and C. methane (CH_4, μmol m^{-2} s^{-1}; n = 21 observations). Standard deviation is plotted as grey bars for both mean diffusive fluxes estimated for two replicates using all k methods (see main manuscript text) and for mean hourly fluxes obtained using the EC. Results are also compared as boxplots for B. CO_2 and D. CH_4 where the mean instantaneous fluxes are plotted as the grey points; the box represents the 25th and 75th percentiles; the median is represented as the bolded line; and the whiskers represent the minimum and maximum values (1.5x interquartile range). Dashed vertical and horizontal lines correspond to zero fluxes; the one-to-one line is plotted as a solid black line.

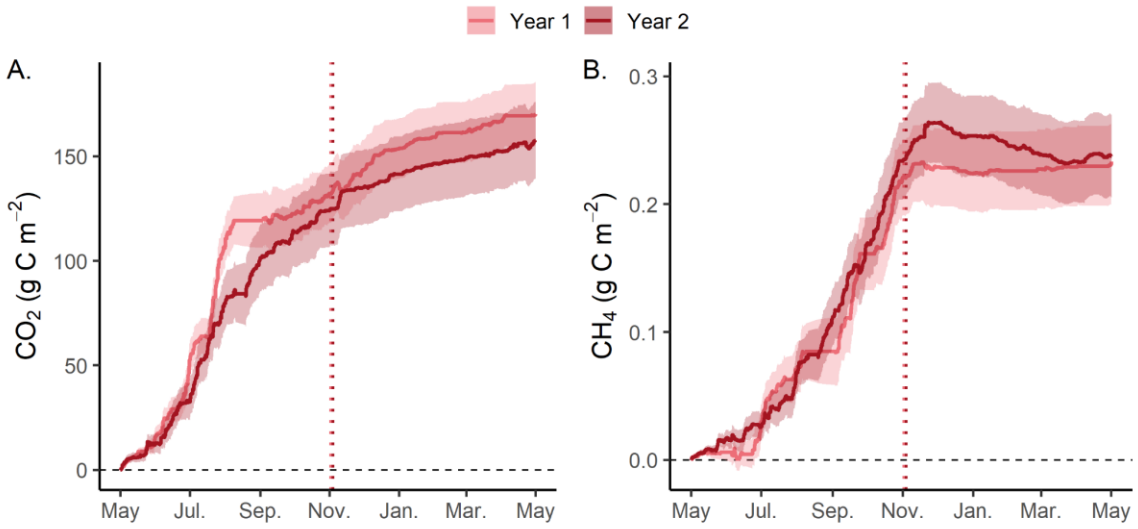

Figure S12. Annual cumulative fluxes for A. carbon dioxide (CO_2, g C m^{-2}) and B. methane (CH_4, g C m^{-2}) using measured eddy covariance fluxes from Falling Creek Reservoir for Year 1 (May 2020-April 2021; pink) and Year 2 (May 2021-April 2022; dark red). Shaded areas correspond to the aggregated standard deviation (±1 S.D.) of measurements. The horizontal dashed line corresponds to zero and the vertical dotted line indicates reservoir fall turnover for both years. Note: these cumulative fluxes only represent 22 and 24% of CO_2 fluxes and 16 and 23% of CH_4 fluxes measured directly using the EC system in year 1 and year 2, respectively. When upscaling to the full year, this would lead to 774 and 657 g CO_2 m^{-2} for year 1 and year 2 and 1.45 and 1.03 g CH_4 m^{-2}, respectively.

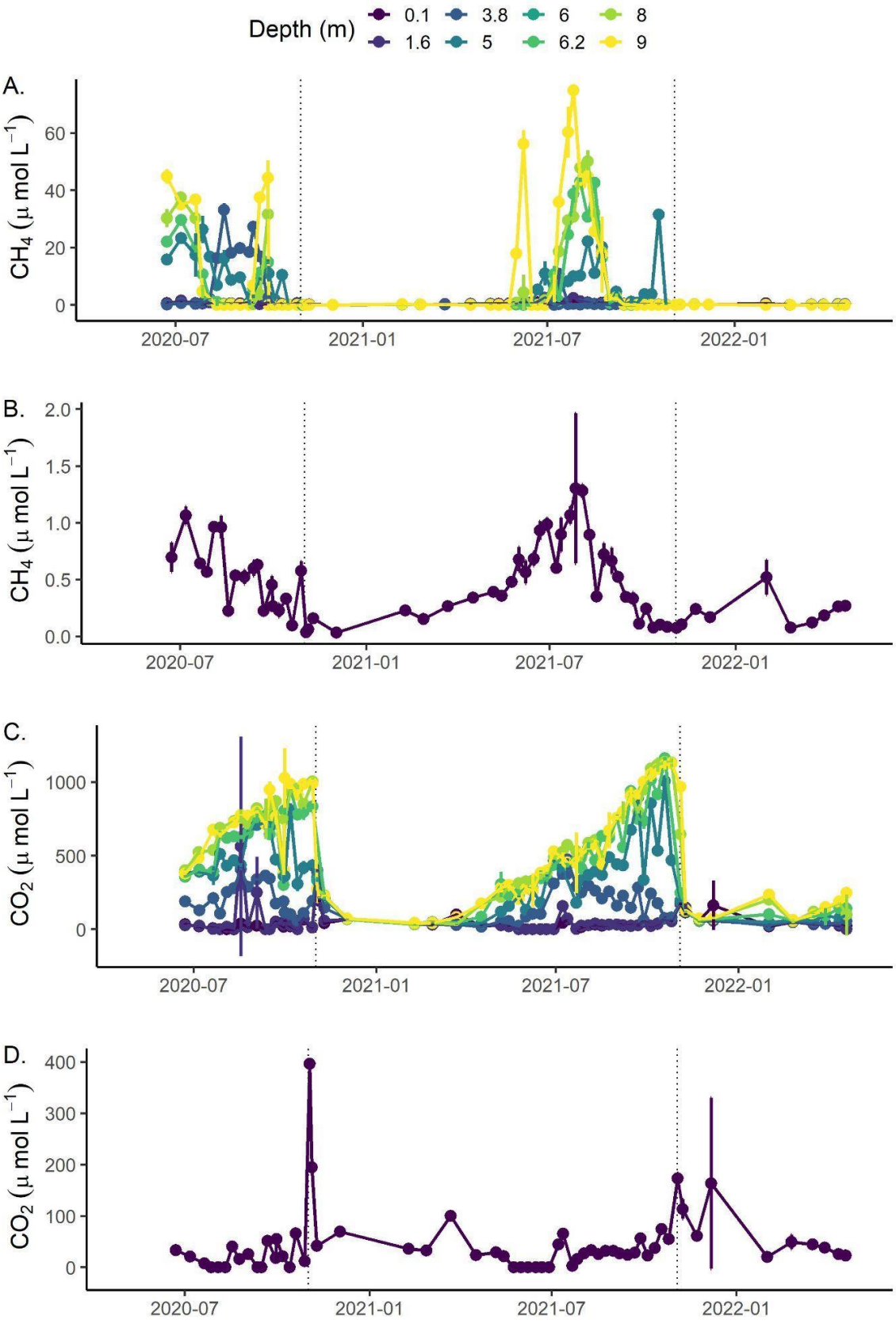
Depth (m)
0.1
1.6
3.8
5
6
6.2
8
9
A.
CH_4 (μ mol L^{-1})
0
20
40
60
2020-07
2021-01
2021-07
2022-01
B.
CH_4 (μ mol L^{-1})
0.0
0.5
1.0
1.5
2.0
2020-07
2021-01
2021-07
2022-01
C.
CO_2 (μ mol L^{-1})
0
500
1000
2020-07
2021-01
2021-07
2022-01
D.
CO_2 (μ mol L^{-1})
0
100
200
300
400
2020-07
2021-01
2021-07
2022-01

Fig. S13. A. Water column dissolved methane (CH_4, μmol m^{-2} s^{-1}) plotted for multiple depths throughout the water column; B. Dissolved CH_4 measured at the surface of the reservoir (0.1 m); C. Dissolved carbon dioxide (CO_2, μmol m^{-2} s^{-1}) measured at multiple depths; and D. dissolved CO_2 measured at 0.1 m. All samples were collected at the deepest point of the reservoir located near the eddy covariance system (EC). The mean and standard deviation of two replicate samples are reported. The dashed, vertical line corresponds to fall turnover for Year 1 and Year 2.

	Percent available CO_2 fluxes (%)	**Percent available CH_4 fluxes (%)**
Raw data available	84	73
Removing fluxes from behind the dam (<80° and >250°)	59	52
QA/QC* of fluxes, LE**, and H***	39	33
Removing fluxes outside of reservoir footprint	29	25
Removing fluxes with low u*	23	19

* QA/QC = Quality assurance/quality control
** Latent energy flux
*** Sensible heat flux

Table S1. Percent of measured carbon dioxide (CO_2) and methane (CH_4) fluxes retained for analysis following data post-processing and various steps of data post-processing. See main manuscript for description of each post-processing step; all code is available in (Carey et al. 2022a).

	Start Date	**End Date**
Intermittent Ice on	10 January 2021	10 February 2021
Intermittent Ice on	11 January 2022	14 January 2022
Continuous Ice on	16 January 2022	10 February 2022

Table S2. Start and end dates used to define intermittent ice-on and continuous ice-on periods during the winter for 2020-2021 and winter 2021-2022 in Falling Creek Reservoir (Carey and Breef-Pilz, 2022).

Parameter	% Missing	R^2	r	Linear equation
Wind speed	12	0.60	0.78	EC = Met*0.50 + 0.19
Air Temperature	39	0.97	0.98	EC = Met*0.95 - 1.01
Sonic Air Temperature	39	0.97	0.98	EC = Met*1.03 - 0.56
Relative Humidity	41	0.75	0.87	EC = Met*0.80 + 13.76

Table S3. Meteorological variables derived from the eddy covariance (EC) system which were estimated with meteorological data obtained from the meteorological (Met) station deployed on the dam of Falling Creek Reservoir. The percent of missing data (% Missing) represents the percent of data missing from the EC system over the two-year monitoring period that was estimated from the meteorological data. The R^2 is included for the linear relationship between the EC and Met data along with the linear equation used for estimation, r denotes Spearman rho correlation. Parameters include: wind speed (m s^{-1}), air temperature (K), sonic air temperature (K), and relative humidity (%).

	Daily						
	DO % Sat.	**Chl-a ($\mu g\ L^{-1}$)**	**fDOM (RFU)**	**Inflow ($m^3\ s^{-1}$)**	**Temp Diff.**	**N^2**	**Thermo Depth (m)**
Surface Temp. (ºC)	0.04	-0.54	0.30	0.02	0.94	0.91	-0.01
DO % Sat.		0.10	0.01	0.39	0.12	0.00	-0.05
Chl-a ($\mu g\ L^{-1}$)			-0.18	-0.16	-0.53	-0.49	-0.02
fDOM (RFU)				0.13	0.23	0.28	-0.05
Inflow ($m^3\ s^{-1}$)					0.14	-0.03	-0.18
Temp Diff.						0.92	-0.17
N^2							-0.15
	Weekly						
Surface Temp. (ºC)	0.10	-0.52	0.18	0.06	0.95	0.93	0.16
DO % Sat.		0.07	-0.07	0.39	0.17	0.06	-0.01
Chl-a ($\mu g\ L^{-1}$)			-0.25	-0.19	-0.52	-0.50	-0.07
fDOM (RFU)				0.11	0.11	0.21	-0.09
Inflow ($m^3\ s^{-1}$)					0.14	0.00	-0.17
Temp Diff.						0.95	0.01
N^2							-0.01
	Monthly						
Surface Temp. (ºC)	0.16	-0.68	0.23	0.03	0.96	0.95	0.03
DO % Sat.		-0.15	-0.14	0.65	0.23	0.11	0.00
Chl-a ($\mu g\ L^{-1}$)			-0.45	-0.18	-0.68	-0.64	0.05
fDOM (RFU)				-0.03	0.16	0.30	-0.04
Inflow ($m^3\ s^{-1}$)					0.13	0.01	-0.27

Temp Diff.						0.96	-0.12
N^2							-0.11

Table S4. Correlations (Pearson's rho) among environmental parameters identified for the ARIMA analyses, including surface temperature (surface temp., °C), percent dissolved oxygen saturation (DO % Sat.), chlorophyll-*a* (Chl-a, µg L^{-1}), fluorescent dissolved organic matter (fDOM, relative fluorescence units, RFU), inflow (m^3 s^{-1}), temperature difference (Temp Diff.) between the surface (0.1 m) and bottom (9 m), and buoyancy frequency (N^2). Highlighted boxes indicate environmental variables which were removed due to collinearity (rho>|0.70|).

		Minimum (μmol m^{-2} s^{-1})	Maximum (μmol m^{-2} s^{-1})	Median (μmol m^{-2} s^{-1})	Mean (μmol m^{-2} s^{-1})	Standard Deviation (μmol m^{-2} s^{-1})	Coefficient of Variation (%)
CH_4	Measured EC	-0.084	0.096	0.001	0.003	0.011	350.571
	Diffusive (Mean)	-0.0059	0.0928	0.0020	0.0048	0.0074	154.62
CO_2	Measured EC	-39.46	52.67	0.79	1.86	6.21	334.21
	Diffusive (Mean)	-1.24	17.50	0.11	0.38	1.22	325.66

Table S5. Minimum, maximum, median, mean, standard deviation, and coefficient of variation for measured methane (CH_4) and carbon dioxide (CO_2) fluxes for the study period (1 May 2020 to 30 April 2022) obtained from the eddy covariance (EC) system and mean diffusive fluxes. Mean diffusive fluxes represent all diffusive methods.

	25th Percentile	Median	75th Percentile	*p*-value
	CO_2 (μmol m^{-2} s^{-1})			
Day	-0.44	1.05	3.91	
Night	-0.60	1.03	3.48	0.093
Dawn	-0.07	1.34	4.37	
Dusk	-0.66	-0.03	0.65	<0.001
	CH_4 (μmol m^{-2} s^{-1})			
Day	-0.0017	0.0013	0.0079	
Night	-0.0016	0.0011	0.0066	0.162
Dawn	-0.0027	0.0002	0.0052	
Dusk	-0.0008	0.0014	0.0062	0.357
	Wind (m s^{-1})			
Day	0.92	1.27	1.73	
Night	0.76	1.03	1.44	<0.001
Dawn	0.95	1.24	1.64	
Dusk	0.87	1.23	1.67	0.003

Table S6. Diel (day/night) and dawn/dusk comparisons for measured eddy covariance (EC) fluxes for carbon dioxide (CO_2, μmol m^{-2} s^{-1}) and methane (CH_4, μmol m^{-2} s^{-1}) along with wind (m s^{-1}). Day corresponds to measurements collected from 11:00 to 13:00 while night corresponds to 23:00 to 01:00 throughout the time period. Dawn corresponds to measurements collected from 05:00 to 07:00 and dusk corresponds to 17:00 to 19:00. Statistically significant differences ($p < 0.05$) based on paired Wilcoxon sign-rank tests are highlighted in grey.

	Year 1	Year 2	Total Study Period
Mean Temp. (°C)	13.8	14.4	14.1
Min. Temp. (°C)	-9.93	-11.5	
Max. Temp. (°C)	35.1	35.0	
Mean Wind Speed ($m\ s^{-1}$)	2.00	1.97	1.99
Max. Wind Speed ($m\ s^{-1}$)	9.28	11.2	
Dominant Wind Direction (°)	191	199	198
Total Rainfall (mm)	1438	790	2228

Table S7. Various climatological variables calculated for Falling Creek Reservoir (FCR) for Year 1 (01 May 2020-30 April 2021), Year 2 (01 May 2021-30 April 2022), and the full study period calculated from the meteorological station deployed at the dam.

	Year 1	Year 2	Total Study Period
Mean Surface Temp. (ºC)	15.2	15.9	15.6
Min. Surface Temp. (ºC)	1.23	1.88	
Max. Surface Temp. (ºC)	31.4	31.3	
Mean Chl-a (µg L^{-1})	11.5	12.3	11.9
Min. Chl-a (µg L^{-1})	1.34	0.25	
Max Chla (µg L^{-1})	90.3	121	
Mean fDOM (RFU)	6.09	6.04	6.1
Min. fDOM (RFU)	3.19	3.01	
Max. fDOM (RFU)	10.4	8.79	
Mean % DO	107	97.8	102
Min. % DO	8.12	0	
Max. % DO	220	208	
Mean Inflow (m^3 s^{-1})	0.056	0.013	0.034
Min. Inflow (m^3 s^{-1})	0.005	0.006	
Max. Inflow (m^3 s^{-1})	0.27	0.20	

Table S8. Mean, minimum, and maximum calculated for key environmental variables from Falling Creek Reservoir during year 1 (May 2020 - April 2021) and year 2 (May 2021 - April 2022) including: Surface temperature, Chlorophyll-a (Chl-a), fluorescent dissolved organic matter (fDOM, RFU), percent dissolved oxygen (% DO), and inflow.

GHG	Order	AR(1)	MA(1)	MA(2)	Temp. Surf. (ºC)	% DO Sat.	Chl-a (µg L^{-1})	fDOM (RFU)	Flow (m^3 s^{-1})	Thermo. (m)	AICc	RMSE
	Daily											
CO_2	(1,0,0)	0.11			0.18		-0.17	0.07	0.08	-0.09	1281.69	0.97
S.E.		0.05			0.07		0.06	0.05	0.05	0.05		
CO_2	(1,0,0)	0.10			0.20	-0.07	-0.14	0.07	0.12	-0.09	1281.79	0.97
S.E.		0.05			0.07	0.05	0.06	0.05	0.06	0.05		
CO_2	(0,0,2)		0.11	0.05	0.20		-0.17		0.08	-0.09	1282.98	0.97
S.E.			0.05	0.05	0.07		0.06		0.05	0.05		
CO_2	(0,0,2)		0.10	0.04	0.22	-0.07	-0.15		0.11	-0.09	1283.35	0.97
S.E.			0.05	0.05	0.07	0.05	0.06		0.06	0.05		
CH_4	(0,0,0)				0.27			0.12		0.25	1213.36	1.02
S.E.					0.05			0.05		0.05		
CH_4	(0,0,0)				0.28	-0.04		0.12		0.25	1214.53	1.02
S.E.					0.05	0.04		0.05		0.05		
CH_4	(0,0,0)				0.28		0.02	0.12		0.25	1215.30	1.02
S.E.					0.07		0.06	0.05		0.05		

GHG	Order	AR(1)	MA(1)	MA(2)	Temp. Surf. (ºC)	% DO Sat.	Chl-a (µg L^{-1})	fDOM (RFU)	Flow (m^3 s^{-1})	Thermo. (m)	AICc	RMSE
	Weekly											
CO_2	(0,0,0)				0.64	-0.16		0.13	0.20	-0.19	183.00	0.63
S.E.					0.07	0.07		0.07	0.08	0.07		
CO_2	(0,0,0)				0.67	-0.17			0.19	-0.20	184.05	0.64
S.E.					0.07	0.07			0.08	0.07		
CH_4	(0,1,1)		-0.75		0.36			0.23	-0.36	0.24	184.13	0.64
S.E.			0.09		0.15			0.10	0.13	0.08		
CH_4	(0,1,1)		-0.65					0.28	-0.43	0.21	185.88	0.65
S.E.			0.09					0.11	0.15	0.08		
	Monthly											
CO_2	(0,0,0)				0.73			0.24		-0.31	42.58	0.48
S.E.					0.10			0.10		0.10		
CO_2	(0,0,0)				0.71	0.15		0.27		-0.32	43.55	0.45
S.E.					0.10	0.10		0.10		0.10		
CO_2	(0,0,0)				0.73			0.27	0.15	-0.26	43.88	0.46
S.E.					0.10			0.10	0.10	0.10		
CH_4	(0,0,1)		0.72		0.74				-0.26	0.21	38.85	0.41

S.E.			0.18		0.14				0.12	0.07		

Table S9. Best-fit results from Autoregressive Integrated Moving Average (ARIMA) showing the top selected model (lowest corrected Akaike Information Criterion, AICc < 2). Models are separated by greenhouse gas (GHG) flux as carbon dioxide fluxes (CO_2) and methane fluxes (CH_4) as well as by timescale (daily, weekly, monthly). Environmental predictors included: Surface temperature (Surface Temp, °C), dissolved oxygen saturation (DO Sat, %), Chlorophyll-*a* (Chl-a, μg L^{-1}), fluorescent dissolved organic matter (fDOM, RFU), inflow discharge (Inflow, m^3 s^{-1}), and thermocline depth (Thermo. depth, m). Model order is specified as (p,d,q) where p is the order of the AR term, d is the order of the integration term, and q is the order of the MA term. Results for all models with 2 AICc of the best fitting model are included. The root mean square error (RMSE) is also reported for each model. Shaded model results are included in the main manuscript (Table 1). S.E. is the standard error.

	25th Percentile	Median	75th Percentile	p-value
	CO_2 (µmol m^{-2} s^{-1})			
Intermittent ice-on (Year 1)	0.12	0.71	1.34	<0.001
Continuous Ice-on (Year 2)	-0.34	0.28	0.93	
	CH_4 (µmol m^{-2} s^{-1})			
Intermittent ice-on (Year 1)	-0.001	0.001	0.004	<0.001
Continuous Ice-on (Year 2)	-0.002	-0.001	0.000	

Table S10. 25th percentile, median, and 75th percentile reported measured eddy covariance (EC) data for carbon dioxide (CO_2, µmol m^{-2} s^{-1}) and methane (CH_4, µmol m^{-2} s^{-1}) fluxes during winter 2020-2021 (year 1) under partial ice-on ('On') and during winter 2021-2022 (year 2) under continuous ice-on. The Mann-Whitney-Wilcoxon test was used to identify medians which were statistically different. Statistically significant relationships are highlighted in grey.

	Season	CO_2 (μmol m^{-2} s^{-1})		CH_4 (μmol m^{-2} s^{-1})		Wind (m s^{-1})	
		Mean	***p*-value**	**Mean**	***p*-value**	**Mean**	***p*-value**
Day	Spring	1.02		0.000		1.19	
Night	Spring	0.82	0.77	0.001	0.57	0.97	0.01
Day	Summer	2.98		0.006		1.30	
Night	Summer	3.14	0.07	0.004	0.12	0.97	<0.001
Day	Fall	0.79		0.005		1.30	
Night	Fall	0.61	0.86	0.002	0.13	1.09	0.005
Day	Winter	0.68		-0.001		1.26	
Night	Winter	0.61	0.32	0.000	0.03	1.23	0.10
Dawn	Spring	1.32		0.000		1.28	
Dusk	Spring	-0.25	<0.001	0.000	0.06	1.30	0.05
Dawn	Summer	3.55		0.005		1.19	
Dusk	Summer	-0.33	<0.001	0.005	0.24	1.08	0.002
Dawn	Fall	1.28		0.003		1.19	
Dusk	Fall	0.10	0.002	0.004	0.48	1.43	0.76
Dawn	Winter	0.70		-0.002		1.35	
Dusk	Winter	0.19	<0.001	0.000	0.04	1.31	0.07

Table S11 Diel (day/night) and dawn/dusk comparisons for measured eddy covariance (EC) fluxes for carbon dioxide (CO_2, μmol m^{-2} s^{-1}) and methane (CH_4, μmol m^{-2} s^{-1}) along with wind (m s^{-1}) for each season (Spring, March-May; Summer, June-August; Fall, September-November; Winter, December-February). Day corresponds to measurements collected from 11:00 to 13:00 while night corresponds to 23:00 to 01:00 throughout the time period. Dawn corresponds to measurements collected from 05:00 to 07:00 and dusk corresponds to 17:00 to 19:00. Statistically significant differences ($p < 0.05$) based on paired Wilcoxon sign-rank tests are highlighted in grey.